Report on the numerical reservoir model used for the simulation of the Los Humeros super-hot reservoir in Mexico

Deliverable 6.3

Report on the numerical reservoir model used for the simulation of the Los Humeros super-hot reservoir in Mexico

Deliverable 6.3

Version 1.0

Paromita Deb, Dominique Knapp, Gabriele Marquart, Christoph Clauser

Contact: Paromita Deb (pdeb@eonerc.rwth-aachen.de)

RTWH Aachen

Work package 6

28.03.2019

Website: http://www.gemex-h2020.eu

The GEMex project is supported by the European Union's Horizon 2020 programme for Research and Innovation under grant agreement No 727550

Table of Contents

List of figures

List of tables

Executive summary

Work Package 6 of the GEMex project aims to characterise the superhot geothermal reservoir of Los Humeros and the engineered geothermal system (EGS) reservoir of Acoculco in terms of fluid and rock properties, heat transfer and flow conditions.

Both Acoculco and Los Humeros are situated in the Trans Mexican Volcanic Belt and are of high interest because of their unconventional geothermal characteristics. In spite of being under commercial exploitation for almost four decades, the superhot reservoirs of Los Humeros still demands research to fully understand the heat source, the geochemistry of the fluid and the interplay between the different fluid pathways. The conceptual geological ideas of both the fields are poorly understood and are subjects of study within GEMex.

This report describes in details the workflow used for creating the numerical model of Los Humeros which is used for simulating the natural steady state behaviour of fluid flow and heat transport of the field. It should be noted that the geometrical models (both regional and local reservoir scale) used for the parameterization are created within a different Work package (WP 3) and a preliminary version of these geometrical models is used for the work presented here. It is well known that the petrophysical properties as well as the heat flow distribution are highly sensitive to changes in structure and hence the structural model imposes a strong uncertainty to the final result of our simulation. Uncertainties in rock properties and fluid pathways are taken care by simulating different scenarios. However uncertainties in the overall structure of the caldera complex i.e., the modelled units and the fault depths and positions still prevails and the reader needs to be aware of the assumptions and uncertainties in input data before using the result presented here.

1 Introduction

The Los Humeros Volcanic Complex (LHVC) is one of the easternmost quaternary collapse calderas of the Trans-Mexican Volcanic Belt (TMVB), located around 260 km east of Mexico City. It is a large caldera complex situated at an elevation of about 2800 masl. Los Humeros is the third largest geothermal field in Mexico with current running capacity of 68 MW (Arellano et al., 2015). The first deep well was drilled in 1982 and the commercial exploitation began in the year 1990. The field is operated by Comisión Federal de Electricidad (CFE). Figure 1 shows the location of the field within the Trans-Mexican Volcanic Belt.

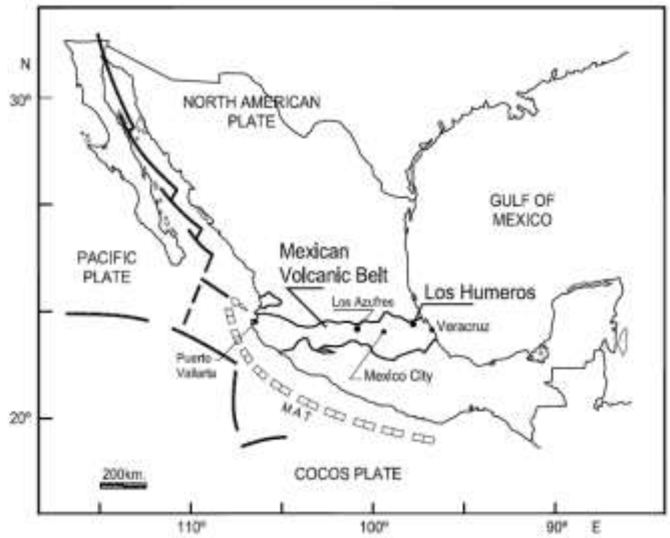

Figure 1: Regional tectonic setting of the Trans-Mexican Volcanic Belt and Los Humeros geothermal field (Arellano et al. 2003), thick black limes are plate boundaries, MAT is location of Middle American Trench

The work is performed within Work Package (WP) 6 and aims to characterise reservoir units of the Los Humeros geothermal system in terms of their petrophysical, thermal and hydraulic properties to an extent permitted by the available data. Geometrical models created in WP 3 and are directly used in WP 6 without further modification. The geometrical model is gridded and geological units are parametrised using data obtained from laboratory measurements performed within WP 6 as well as literature information. The parameterised model is then numerical simulated by solving the heat transfer and fluid flow equations in order to estimate the initial natural state of the Los Humeros field before exploitation. It is important to note that conceptual ideas regarding heat source, fluid pathways, rate of recharge, etc., are still being controversially discussed and hence we need to make certain background assumptions and investigate the temperature behaviour of the field by simulating possible scenarios for heat sources and boundary conditions.

The work area of WP 6 is on a reservoir scale (9.5 x 12.5 x 6.5 km^3) and is much smaller in extent than the regional model (56 ×36 ×12 km^3). Critical conceptual information such as recharge condition, heat source, fluid pathways, etc., required for modelling the natural state conditions of Los Humeros were not available when work began. In view of this, it was necessary to work on a larger scale to develop reasonable estimations of boundary conditions for the reservoir model. Additionally, the reservoir model boundary is cut very close to the Los Humeros caldera fault system. In a convection model, the advective nature of this annular fault will influence the boundary conditions of the reservoir model. The above reasons led us to work on the regional scale initially followed by a more detailed reservoir scale model. This report focus on the following topics:

i. Estimation of boundary conditions for numerical modeling
ii. Parameterization of lithological units

2 Available Data

A collection of literature is available on Los Humeros to provide an initial understanding of the field. In addition, Comisión Federal de Electricidad (CFE) provided an extensive collection of temperature and pressure data for almost 50 wells of Los Humeros. This data provides us the basis for calibration of our models. Figure 2 shows the location of the CFE geothermal wells in the Los Humeros field. The grey dashed lines in the figure indicate the main fault systems of Los Humeros.

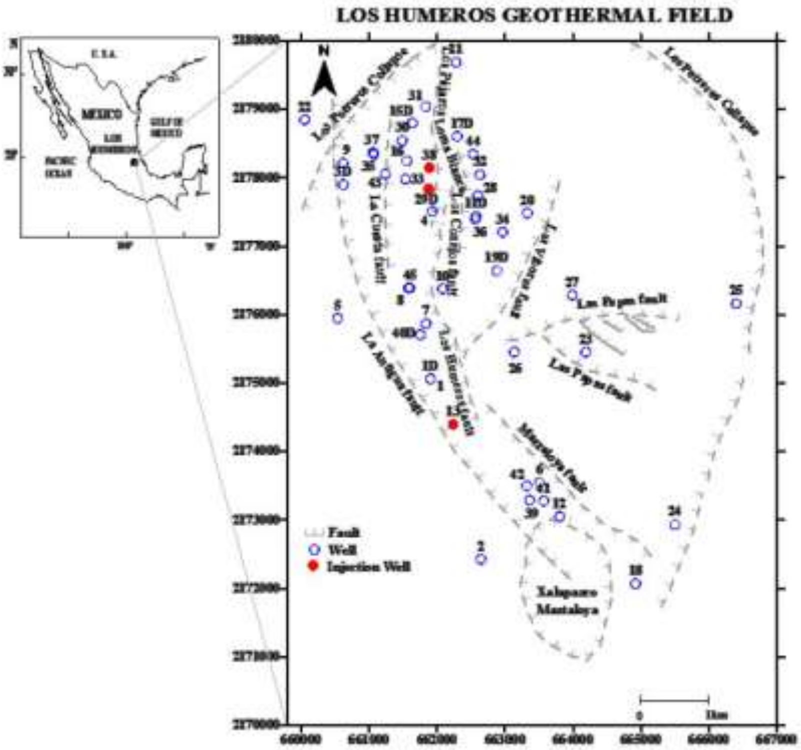

Figure 2: Location of geothermal wells and main fault systems in Los Humeros field (Arellano et al. 2015).

2.1 Well data

2.1.1 Temperature and pressure data

Comisión Federal de Electricidad (CFE) provided data from almost 52 wells which were used as primary information for the purpose of modeling to constrain temperature-depth distribution. The data obtained from CFE were in the form of excel sheets. The data for each well contains the following information:

- well location, interpreted lithology from drill cuttings, well diagram and deviation survey, information on zones of circulation loss and completion tests if available,
- transient temperature and pressure surveys after drilling, normally after 4 hours, 8 hours and 12 hours,

- temperature and pressure surveys conducted during heating up with intervals in the order of days or weeks or months,
- temperature and pressure data measurement (for some wells) in flowing conditions
- production data (of some wells) which included well head pressure (WHP), separation pressure, brine flow, steam flow, mass flow and enthalpy.

In absence of any other stable temperature measurement, the only data available for Los Humeros wells are the temperature logs run after drilling. However, these data collected after drilling and in some cases during heating up surveys are affected due to many factors such as circulation of mud, drilling technology, well radius and, more importantly, communication between the feed zones at different levels. Therefore this unstable temperature data obtained from logging cannot be used as direct indicators of formation temperature. In order to have reliable temperature estimates, a very long shut-in time is required which is not very economical for the operators. In case of Los Humeros, the wells are not only affected due to drilling mud circulation but as well due to strong interflow between the feeding zones. Temperature data for the bottom-hole depth obtained from different runs are used to obtain information about static temperature at different depths.

We used two different methods to correct temperature data and compare the different methods. One of the most widely used method is adapted from Horner (1951) due to the apparent similarity to the conventional pressure build up. Horner's method requires mud circulation times as inputs. For Los Humeros wells, the mud circulation times are not available for most wells and therefore an assumption of 4 hours was made for applying the correction.

Horner's method is described by the following equation:

$$\mathrm{T_{ws}} = \mathrm{T_i} - \mathrm{C}\log\left(\frac{\mathrm{t} + \mathrm{tc}}{\mathrm{t}}\right), \tag{1}$$

where T_{ws} is the shut-in temperature at time t, T_i is the stabilised formation temperature at infinite shut-in time and tc is the mud circulation time.

In Horner's method, the thermal effect of drilling is approximated by a constant linear source (Dowdle and Cobb, 1975). This model describes a straight line with slope m and intercept T_i. T_i is obtained by extrapolation to infinite shut-in time. It has been however suggested that a Horner analysis of temperature build up always underestimates the static formation temperature (Dowdle and Cobb, 1975; Eppelbaum and Kutasov, 2006) and is justified only with certain basic assumptions.

In addition to the Horner analysis, we used another method to estimate the undisturbed formation temperature. This method is based on a conceptual model with an assumption of spherical radial heat flow at the bottom of the well. The mathematical model and the related assumptions are described in Ascencio (1994). The Spherical Radial Heat Flow (SRF) method is based on the following equation

$$\mathrm{T_{ws}} = \mathrm{T_i} - \mathrm{C}\frac{1}{\sqrt{\mathrm{t}}}\ , \tag{2}$$

A plot of shut-in temperature T_{ws} versus the inverse of the square root of shut-in time describes a straight line with slope m and intercept, T_i (the static formation temperature at infinite shut in time).

For Los Humeros wells, it is observed that the temperatures calculated using Equation 2 are higher than the values obtained from Horner's method (Equation 1). Garcia-Gutierrez (2002) suggested that equation 2 provides static temperatures that are closer to the true formation temperatures in the Los Humeros geothermal field. Temperatures corrected using both methods for bottom-hole depth for the Los Humeros wells are presented in Table 1. As these corrected temperatures serve as a critical information towards verification of the numerical model of Los Humeros, we use temperatures obtained from both equations as bounding limits for calibrating our numerical model at bottom hole depth of wells. The lower bound is defined by corrected temperature from Horner's method while temperatures obtained from equation 2 (SRF) is used as the upper bound.

It should be noted that not all Los Humeros wells are used for calibrating our model. The commercial exploitation of the field began in the year 1990. Wells drilled after that period have not been used for calibration.

2.1.2 Petrophysical logs

Out of 52 wells, only two wells had some lithology logs run for a very limited depth interval. In well H 42 and H 43, a suite of measurements consisting of natural gamma ray, density, neutron, resistivity and self-potential. For H 42 the logging depth was between 1220 m and 2200 m whereas in H 43 the lithology measurements were performed between 1245 m and 1620 m. In addition, Full-bore Formation Micro imager (FMI) logging and Dipole Shear Sonic Imager (DSI) were also run in H 43 for two depth intervals with an objective of visualising fractures present in limestone. The first depth interval was between 1250 m and 1633 m and the second between 1711 m and 1813 m. The measurements for the second interval is incomplete due to tool damage at that depth. Deeper measurements were not possible due to high temperatures encountered in the well (Pulido, 2008).

2.1.3 CFE Core data:

In order to perform petrophysical measurements on reservoir samples, plugs from CFE cores were drilled. 64 plugs were obtained from 35 core section of 14 Los Humeros wells. The plugs drilled belonged mostly to the andesite section with few samples of marble and basalts available for new measurement. Details of measurements are available in Deliverable Report D 6.1.

2.2 Outcrop samples

Several field campaigns were conducted between January 2017 and May 2018 to collect representative samples from Los Humeros, Acoculco and the exhumed system, Las Minas. Details of the field campaign, description and physical condition of the samples, methodologies and measurements are described in Deliverable Report D 6.1. The reporting deadline for D 6.1 as well as D 6.2 and D 6.3 were identical. Considering this, it was decided to use measurements performed until November 2018 for petrophysical characterization.

Table 1: Bottomhole temperatures corrected using two different methods for Los Humeros wells

Wells	X	Y	Elevation	Depth of correction	Reduced level	Stabilised	Horner	SRF
			(m.a.s.l.)	(m)	(m.a.s.l.)	(°C)	(°C)	(°C)
H-1-D	661906	2175064	2828	1815	1013		237.38	268.61
H-2-V	662646	2172435	2896	2298	598		277.72	297.4
H-3-V	660622	2177903	2755	1659	1096		274.38	326.87
H-5-V	660540	2175950	2754	1845	909		231.65	251.69
H-6-V	663508	2173545	2894	2540	354		316.35	348.92
H-7-V	661838	2175871	2782	2281	501		300.84	337.22
H-8-V	661582	2176392	2771	2300	471		394.03	456.99
H-11-D	662574	2177436	2812	1460	1352		281.33	310.29
H-13-D	662244	2177406	2835	1850	985		268.26	288.84
H 13-V	662244	2177406	2835	2401	434		303.43	329.64
H-14-V	663832	2169627	2815	1373	1442		116.5	144.08
H-16-V	661557	2178250	2783	2038	745		318.16	369.36
H-18-V	664916	2172077	3002	2885	117		294	332.02
H-21-V	662279	2179691	2871	2214	657		276.16	300.7
H-22-V	660055	2178853	2763	1539	1224		268.81	297.95
H-24-V	665497	2172938	2922	3263	-341		259	288.05
H-25-V	666393	2176169	2800	2283	517		194.63	223.32
H-28-V	662601	2177741	2819	2558	261	361		
H-29-D	661884	2177843	2807	2186	621	352		
H-31-V	661832	2179041	2810	1914	896		315.67	349.97
H-32-V	662631	2178043	2818	2186	632		332.13	362.97
H-38-V	661897	2178155	2795	1390	1405		166.23	189.76
H-39-V	663365	2173291	2890	2495	395		255.31	286.89

3 Geological model:

3.1 Regional geology:

Los Humeros caldera system is in general characterized by a quaternary basalt-andesite-rhyolite volcanism. It is located at the northern end of a 40 km-wide NNE-SSW depression (Serdán Oriental Basin) characterized by bimodal, mainly monogenetic volcanism (Norini, 2015). The system is limited to the east by the active Coffre de Perote Volcanic chain, which hosts active andesite stratovolcanoes and dome complexes (Carrasco-Núñez et al., 2017) and to the west by the Sierra Madre Oriental highs fold and thrust province (Norini, 2015). In the area, the volcanic rocks overlie an intrusive, metamorphic and sedimentary sequence made up by a Late Paleozoic crystalline complex composed of green schists, granodiorites and granites (Carrasco-Núñez et al., 2017) and a Triassic-Cretaceous series of limestones and terrigenous sedimentary rocks of less than 3000 m thickness (Norini, 2015 and references therein). The sedimentary limestone basement is highly deformed and shows large overthrusts along the edges of the massive carbonate platforms, where deformation is mainly controlled by the lithology and the thickness of the Cretaceous formations (Suter, 1984; Roure et al., 2009). Due to Tertiary intrusions of granodiorite and syenite, the Cretaceous limestones are locally metamorphosed to marble, hornfels and skarn (Carrasco-Núñez et al., 2017; Norini 2015).

The sedimentary basement of Los Humeros is overlain by thick andesite sequence of Upper Miocene age (10 Ma), which ranges in thickness from 800 m to more than 1200 m as encountered in many CFE wells. This correlates well with the Cuyaoca Andesite and the Alseseca Andesite (Norini, 2015; Lopéz-Hernandez, 1995). This andesite sequence is mainly composed of hornblende rich andesites and basaltic lava flows. This sequence is overlain by a vitric tuff unit called Toba Humeros which is mainly composed of altered and low permeability silicic deposits (Arellano et al., 2003). Although it is identified in many CFE wells with thickness between 150 m to 200 m, it has not been encountered as outcrop. Between 5 Ma and 1.5 Ma, another andesite sequence was emplaced which belongs to the Teziutlan volcanic unit. The sequence varies in thickness between 700 m to 900 m as observed in the geothermal wells of CFE and forms the basement of the LHVC.

This volcanic complex comprises of at least two main caldera forming phases, resulting in a nested caldera system. The first stage comprises of eruption of pre-caldera rhyolitic lava domes and are dated at 0.47 ± 0.04 Ma (Ferriz and Mahood, 1984). Following this phase, a huge emission of pyroclastic lava took place which covered an area of 3500 km^2. These led to the emplacement of Xaltipan Ignimbrites with an estimated volume of 115 km^3 and caused the collapse of the volcanic complex giving rise to the Los Humeros caldera. The original dimensions of the caldera is around 21 km × 15 km (Ferriz and Mahood, 1984). The caldera complex is estimated to have had a 450 m collapse based on the observation of the offset of the lower contact of the ignimbrites. This estimation corresponds well to the volume of the Xaltipan ignimbrites (Ferriz and Mahood, 1984). A number of high-silica rhyolitic domes were emplaced after this process which were later covered discordantly by the Faby Tuff (Ferriz and Mahood, 1984). These rhyodacitic tuffs represents a volume of 10 km^3 of magma and is dated at 360 ka and 240 ka. This was followed by the second caldera collapse event which led to the formation of the Los Potreros caldera which is 8 km to 10 km wide. This event is dated 100 ka and approximately 12 km^3 of magma was released (Ferriz and Mahood, 1984). The last caldera forming event took place at around 40 ka consisting of eruption of basalts, rhyodacites and andesites. During this cycle a small sub-plinian eruption gave rise to El Xalapsco, the smallest caldera within Los Humeros caldera compex with a diameter of around 1.7 km. This is located in the southern sector of Los Potreros caldera.

The resulting stratigraphy of the caldera complex was described in detail by Norini (2015) and Carrasco-Núñez et al. (2017). An overview of the regional geological setting is given by the revised geological map (Figure 3) from Carrasco-Núñez et al. (2017).

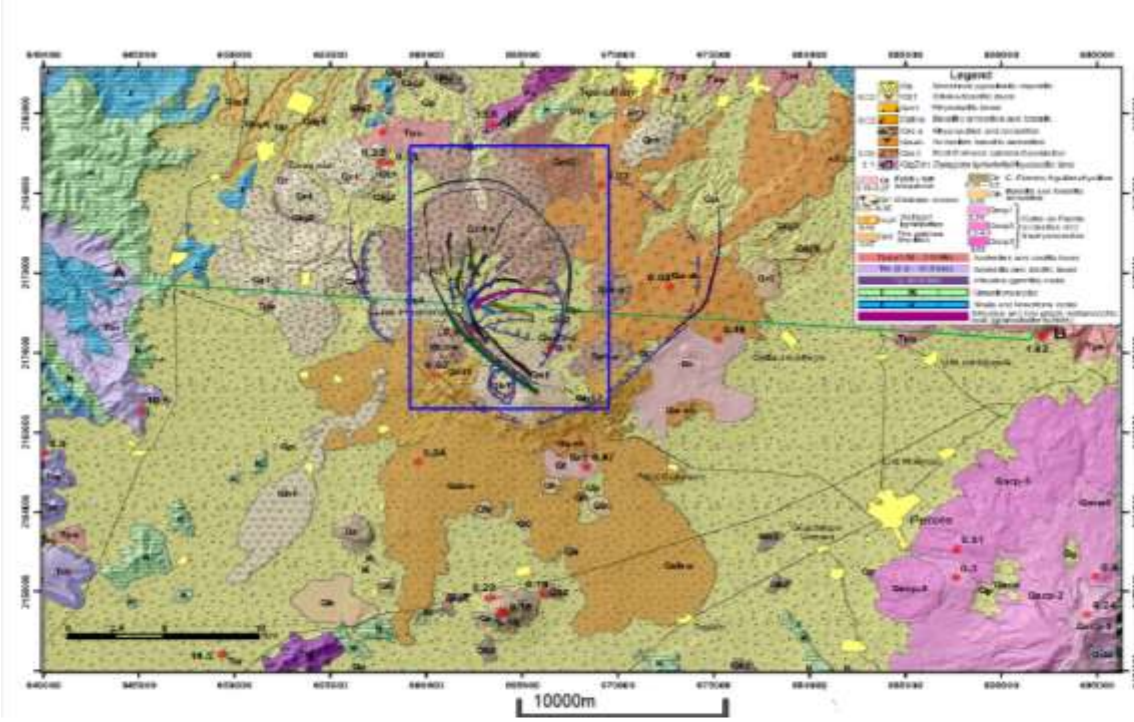

Figure 3: Revised regional geological map of the Los Humeros Caldera Complex (Carrasco-Núñez et al. 2017); the blue outline indicates the boundary of the local reservoir model.

3.2 Modeled Geological Units

The Los Humeros area was modelled at two scales: a regional one dedicated to the understanding of the geothermal system, and is modelled within the extent of the above geological map (Figure 3) and a local model focusing on the area under exploitation by CFE and is shown by the blue boundary in the same map. This model was constructed mainly from the data obtained from sixteen CFE wells with geological description, geological map from Carrasco-Núñez et al. (2017b) and two geological sections from Carrasco-Núñez et al. (2017a) and Norini et al. (2015). Detail description on construction of the Los Humeros geometrical models is available in Calcagno et al. (2018).

The regional model has a dimension of 56 x 36 x 12 km^3 and reaches a depth of 7 km below mean sea level. It is divided into four major groups representing the major events during the evolution of the caldera system (Table 2). These groups comprise the pre-volcanic basement comprising limestone and crystalline basement, the pre-caldera group, built by the andesite sections, the caldera group, mainly composed of ignimbrites and the post-caldera group, comprising different volcanic and alluvial deposits. The deepest well in drilled in Los Humeros is H-24 which is located at the south-eastern boundary of the field and reaches a depth of almost 341 m below sea level. Below this level, the type of rocks and their petrophysical composition and physical properties remain uncertain. Since no reliable information about the rocks and the nature and position of the heat source driving the volcanic activity in Los Humeros is available, we reduce the vertical extent of the model to 4600 m below sea level and model the heat source as a boundary condition. This also reduces the number of nodes of the numerical model and saves computation time.

In addition, we distinguished the basement group into two subgroups, sedimentary limestone and the crystalline basement part (Table 2, Figure 4). This was done to account for the different thermal and hydraulic properties of the two groups which are modelled together as Group IV in the regional model. The thickness of the limestone basement was estimated not to be larger than 3000 m in the area of Los Humeros (Norini, 2015). From the lithology record of well H-24 we know that in the bottom-hole depth at 340 m below sea level limestone is still encountered. Due to lack of any other information on the exact border between crystalline and sedimentary basement, we separated both groups at a depth of 600 m below mean sea level taking this information into account.

Table 2: Modelled units in Geomodeller (WP3), for numerical modelling, we divided Group IV into two subgroups as indicated in the table - limestone and crystalline basement complex

Groups	Units	Rock description	Age (Ma)
Group I: Post-caldera volcanism	U1 Undefined pyroclastic	Tuffs, pumices, & some alluvium	< 0.003
	U2 Post caldera	Rhyodacites, andesites, basaltic andesites, and olivine basalts lava flows, with ages between	0.05 and 0.003
Group II: Caldera volcanism	U3 Los Potreros caldera	Rhyodacitic flows and Zaragoza Ignimbrites	0.069
	U4 Intermediate caldera	Faby Tuff & andesitic-dacitic lava flows (0.27 to 0.19 Ma)	0.07
		Rhyolitic and obsidian domes (0.36 to 0.22 Ma)	0.074
	U5 Los Humeros caldera	Mainly the Xaltipan Ignimbrite with minor andesitic and rhyolitic lavas (Quaterny)	0.165
Group III: Pre-Caldera volcanism	U6 Upper pre-caldera	Rhyolites, dacites, some andesites and tuffs and minor basalts	0.693 to 0.155
	U7 Intermediate pre-caldera	Mainly pyroxene andesites (Teziultán Andesites) with mafic andesites in the basal part and/or dacites (Plio-Quaternary)	2.61 to 1.46
	U8 Basal pre-caldera	Mainly hornblende andesites (Alseseca Andesites & Cerro Grande) and dacites - Miocene	10.5 to 8.9
Group IV: Limestone Basement	U9 Basement	Middle Miocene granitic intrusions	15.12
		Cretaceous limestone and shales and minor flint	~140
		Jurassic limestones and shales	~190
Group IV: Crystalline Basement	U10 Basement	Paleozoic granites and schists (Teziultán Massif)	> 251

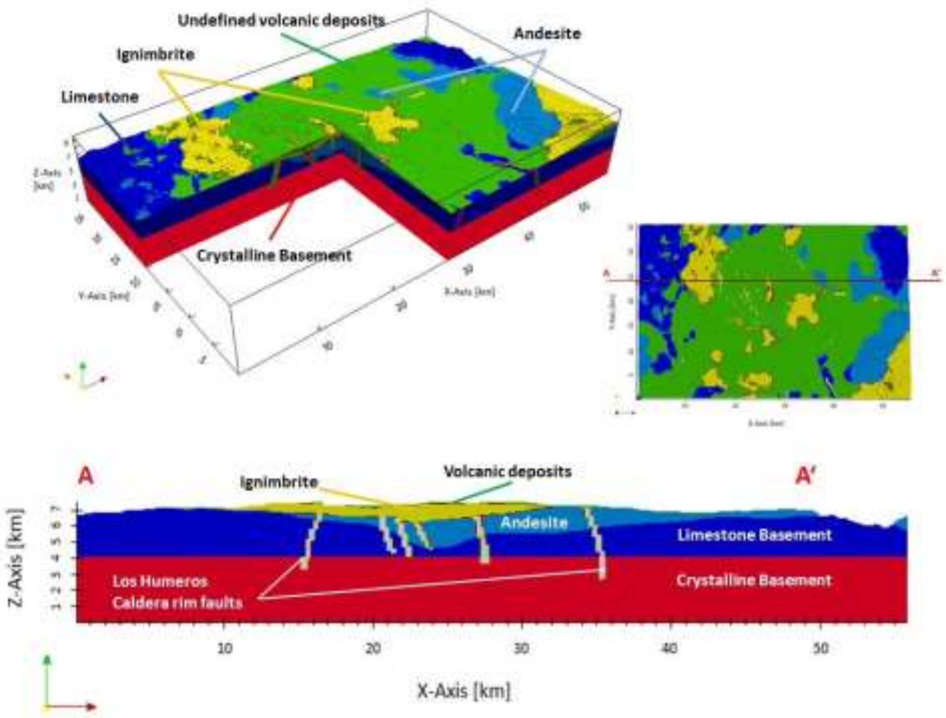

Figure 4: Unit configuration of the regional model for the Los Humeros caldera, comprising 4 chronological groups, presented in the geological section (Table 2). For the SHEMAT model we distinguish additionally between limestone and crystalline basement complex

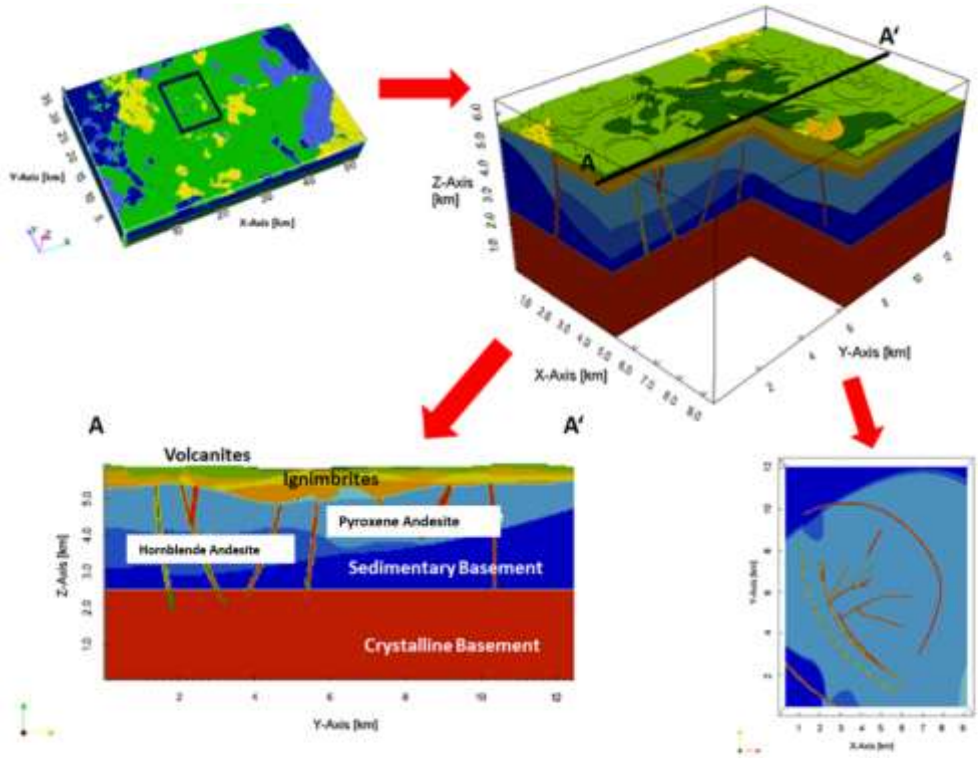

Figure 5: Unit configuration of the reservoir model of Los Humeros Geothermal field (outlined by the blue boundary in Figure 3), comprising 9 geological units (differently coloured in the cross-section) and 20 main fault structures (Slice on the right side taken at 1500 m.a.s.l.)

The reservoir model provided by WP 3 has a size of 9.5 x 12.5 x 12 km^3 and comprises of 9 units: basement, basal pre-caldera, intermediate pre-caldera, upper pre-caldera, Los Humeros caldera, intermediate caldera, Los Potreros caldera, post-caldera, and undefined pyroclastic rocks (Table 2). For modeling purpose, the basement of the reservoir model is divided as well into two groups similar to the regional model: sedimentary limestone and crystalline basement which results in 10 lithological units for the local reservoir model (Figure 4 and Figure 5). The depth of the model is limited to 1.5 km below sea level.

3.3 Conceptual model

The volcanological conceptual and hydrogeological model of Los Humeros in the regional scale is an output of WP 3 and therefore is currently not available to WP 6. However in order to work on the local scale model, it is important to have the knowledge of the boundary conditions which must be extracted from a model of a larger scale. Therefore, at WP 6 we performed simulations in the regional scale to extract pressure and temperature boundary conditions for every boundary node of the reservoir scale model. The conceptual idea regarding several aspects of the geothermal system like heat source, recharge pathways, etc., are still unclear, we therefore test different scenarios to understand the natural state of the fluid and heat transport system in Los Humeros.

Heat source (WP 3, Inputs from Guido Giordano, UNIROMA3): From the available literature the conceptual model of the heat source below Los Humeros Caldera has commonly been regarded as a single cooling, partially crystallized magma chamber. This is inferred from the main caldera-forming eruption which occurred at 160 ka and emplaced the 100 km^3 Xaltipan ignimbrite (Ferriz and Mahood, 1984). The magma chamber/heat source has been previously modelled at a depth of about 4 km to 7 km below surface (based on mineral geobarometers (Verma, 1985), with the same lateral extension as the Los Humeros caldera. Originally of olivine basaltic composition, the magma chamber is considered to be chemically stratified based on crystal fractionation and assimilation modelling (Ferriz and Mahood, 1984). An initial emplacement temperature of 1350 °C is suggested by Verma et al. (2011).

New detailed volcanological and petrological studies conducted during the GEMEX Project (WP4 and WP3; Giordano et al., 2018) are now questioning the previous conceptual model based on the following evidence:

1) The post-caldera volcanism is characterized by scattered monogenetic centers along and around the caldera floor, each characterized by different chemistry, spanning from olivine-basalt to trachyte and rhyolite, with no clear spatial nor temporal pattern or trend. This rules out the possibility of a single magma chamber existing below the caldera and being the source region for these different volcanic products. In contrast, this observation suggests the existence of several small magma batches, each undergoing independent evolution through crystal fractionation, likely set in a larger and more extensive crystal mush related to the preceding magmatic history.
2) New geothermometric and geobarometric data retrieved from all the relevant post-caldera volcanic units indicate a polybaric evolution for the Los Humeros magmas, with the shallowest ponding areas at depth comprised between 5 km and the surface.
3) The variable chemistry of magmas also indicate that the temperature of the post-caldera heat sources might also vary.

In summary the new data clearly depict a new conceptual model for the Los Humeros heat source characterized by a “granular” geometry made of several small batches of magma, emplaced at different times during post-caldera volcanism, and different depths and progressively cooled before they could coalesce to form a larger magma reservoir. In particular magma batches embedded above 5 km depth are of interest for heating of geothermal fluids and have to be considered in geothermal modelling.

The exact depth, temperature, cooling and recharge history, as well as the shape and the position of each of those magma pockets is still a subject of investigation within GEMex.

In addition, the high variability in the bottom-hole temperatures encountered in different wells, which are within few kilometers apart, does not support the idea of a single magma chamber at shallow depth.

Reservoir rocks: Existence of two feeding zones of reservoir fluids have been proposed based on the temperature, pressure records from different wells, fluid geochemistry profiles and drill cuttings: the upper zone is composed of dominant liquid with hydrostatic pressure profile and neutral pH, while the lower one being steam dominated with steam static pressure profile and much lower pH (Cedillo-Rodríguez, 2000; Gutierrez-Negrin, 2010). The upper zone occurs in the augite andesite and the lower one in the Tezuitlan hornblende andesite. Cedillo- Rodríguez (1997) proposes that both the layers are separated by low permeability vitreous tuff called Toba Humeros, while Gutierrez-Negrin (2010, and references therein) indicates that these are not two separate reservoirs but rather structurally controlled feeding zones originating from the same reservoir. The low pH fluid at deeper depths is explained as a result of a post-exploitation process induced due to extraction of fluids by (Izquierdo et al., 2000; Gutierrez-Negrin, 2010). In addition, according to Gutierrez-Negrin (2010) there is no registered volcanic episode which could have deposited the tuff layer between 10 Ma and 3.5 Ma.

Hydrogeological Situation: From regional studies of hydrogeology, hydrochemistry and structural geology it was concluded that the shallow groundwater layers of the surrounding area do not have a hydraulic connection to the deep geothermal wells, springs or water wells within the caldera (Cedillo Rodríguez, 2000). The deep annular faults of Los Humeros and Los Potreros form impermeable barriers to lateral recharge. Therefore it is proposed that the main recharge takes place vertically through rainfall infiltration within the caldera. The basaltic flows which forms the post caldera volcanic deposits have a moderate capacity of water infiltration and may act as shallow aquifers. However, the presence of two extensive low permeable ignimbrite layers limits the infiltration vertically as well causing insufficient recharge to the geothermal system. Lack of recharge results in pressure depletion within the reservoir which explains the production of very high enthalpy fluids from the geothermal wells. This is explained in Arellano et al. (2015) using production data from many geothermal wells. Movement of magmatic fluids upward vertically through faults and fractures has also been suggested as a possible recharge option (Cedillo Rodríguez, 2000)

Reecently, another possible recharge situation has been under discussion at a regional scale. Over-thrusted sedimentary sequence of limestones are observed in the outcrop scale. These highly fractured limestones can act as preferential pathways if connected through regional fault planes, creating possible pathways for distal lateral recharge. New studies expect the origin of the recharge to be meteoric and distal with a general flow path pattern from N-W to S-E. This idea was obtained from the chemical composition of the water and the isotopic fingerprint, resulting from initial isotopic composition, chemical rock-water interactions and relative isotopic composition changes due to liquid-steam phase changes. Further geochemical studies of the fluids are required in order to confirm the depth at which this lateral recharge if at all infiltrates the caldera complex.

In general, both cases, distal lateral recharge, as well as an isolated caldera system sealed by closed caldera faults are possible. However the amount of recharge happening in both cases seem to be not sufficient for maintaining pressure balance within the reservoir. In Section 4.2.4, we present simulations performed by assuming different permeability scenarios for limestone by upscaling intrinsic limestone permeability by several magnitudes to evaluate the effect on the flow field.

4 Numerical model

The numerical model is based on a geological structural model which is created in WP 3 and briefly described in Section 3.2.

4.1 Basic mathematical model equations

For numerical simulation the finite differences code SHEMAT-Suite (Rath et al., 2006) is used. SHEMAT–Suite is based on SHEMAT (Simulator for Heat and Mass Transport; Clauser, 2003) and solves the coupled steady state or transient equations for groundwater flow, heat and reactive solute transport. For our modelling of the natural state of Los Humeros geothermal field, we restrict ourselves to a steady state modelling of the initial temperature and pressure fields, due the unclear conceptual model ideas of the heat source and the lack of information corresponding to the cooling history, the position and the size of possible magma chambers or pockets, which are needed for performing a detailed transient modelling of the fields initial state. This workflow implies to assume the system to be in equilibrium state before production.

The steady state mass conservation of water in a porous medium is expressed by the continuity equation, where h represents the hydraulic head, Q labels the source and sink term, $\boldsymbol{k}$ is the permeability tensor, ρ_f and μ_f are density and dynamic viscosity of the pore fluid, respectively and g represents the gravity acceleration,

$$\nabla\left(\frac{\rho_f g}{\mu_f}\boldsymbol{k}\,\nabla h\right) + Q = 0 \tag{3}$$

The physical properties of water in sub-critical and super-critical conditions are calculated using the correlations provided by the International Association for the Properties of Water and Steam (Wagner et al. 2000). The pore water pressure (P) is calculated according to the head distribution and the depth z, given by the definition of de Marsily (1986), where P_0 represents the pressure at the surface for z=0:

$$P(z,h) = P_0 + \int_0^z \rho_f(\tilde{z})g(h-\tilde{z})d\tilde{z} \tag{4}$$

Heat transport due to conduction, advection and radiogenic heat production is expressed in the energy conservation equation in steady state

$$(\rho c)_f \mathbf{v}\,\nabla \mathrm{T} - \nabla\,(\lambda_e \nabla T) = A \tag{5}$$

The equation consists of an advective term, yielding Darcy velocity **v**, fluid density ρ_f and fluid specific heat capacity c_f, a diffusive term, comprising the effective thermal conductivity of the rock-fluid mixture λ_e and a heat production term A.

Groundwater flow and Darcy velocity **v** are described by the Darcy's Law:

$$\mathbf{v} = \frac{k}{\mu_f}(\nabla p - \rho_f g) \tag{6}$$

Observations of production data from numerous wells of Los Humeros shows that the field was liquid dominated prior to its commercial exploitation. It is estimated that in the beginning of 1990, the liquid saturation was about 90% which decreased to 50% in 2012 (Arellano, 2018) due to lack of sufficient recharge and hence considerable pressure depletion. Therefore, we consider an initial liquid dominated reservoir and account for the supercritical conditions of water in the deep part of the reservoir by calculating the physical properties of water using the correlations by the International Association for the Properties of Water and Steam (Wagner et al., 2000).

Rock thermal conductivity depends on the rock type but generally decreases with temperature (Zoth and Hänel, 1988). It is important to know the representative values of thermal conductivity with temperature and pressure for thermal modelling. In Los Humeros model, however there exists several rock types which are grouped together into one unit and hence it is difficult to isolate the influence of each rock type, i.e. to determine the effective thermal conductivity. The dominant part of the regional model domain is made up by limestone basement intercalcated with shales and metamorphosed to skarn and marble in the contact aureoles. This is overlain by igneous and metamorphic rocks (pre-caldera and caldera deposits). On the reservoir scale model, the relative contribution of metamorphic and igneous rocks are more than the limestone deposits. Lee and Deming (1998) propose that the best theoretical fit for the temperature dependency of igneous and metamorphic rocks in the temperature range from 0°C to 500°C, compared to measurement data is the relationship proposed by Sekiguchi (1984) (7). We used the correction proposed by Sekiguchi (1984) to account for the dominant igneous and magmatic rock compounds within the model domain.

The formula implements the temperature correction for matrix thermal conductivity λ_m on basis of a given matrix conductivity at room temperature $\lambda_{m,0}$ and the temperature T and was included in the manner of Pasquale et al. (2017):

$$\lambda_m = 1.8418 + (\lambda_{m,0} - 1.8418)(\frac{1}{0.002732\,T + 0.7463} - 0.2485) \tag{7}$$

Effective thermal conductivity of the fluid filled porous rock λ_e is dependent on porosity Φ, fluid thermal conductivity λ_f and rock matrix thermal conductivity λ_m. It is calculated according to the geometric mean (Clauser, 2003):

$$\lambda_e = \lambda_f^{\phi}\,\lambda_m^{(1-\phi)} \tag{8}$$

4.2 Parameterization

The reservoir model which is defined by the blue boundary in Figure 3 is the study area for WP 6. However, in absence of any temperature and pressure information around the caldera, it is not possible to define any boundary conditions for the local reservoir model. Additionally, the structural uncertainties due to under-determined configurations of the caldera annular fault structures makes it difficult to understand the heat exchange processes within the subsurface. The only set of information available includes the temperature data at the well bottom within the local model boundary. Therefore, the bigger regional model boundary is considered for initial simulations to extract boundary conditions and understand the impact of structural uncertainties and heat flow configurations on the local reservoir model boundary.

4.2.1 Discretisation

The reduced regional model comprises a horizontal size of 56 km by 36 km with a vertical extent of 9.6 km. Cell sizes have been kept constant to a size of 250 m by 250 m by 50 m for each cell. The higher vertical resolution was chosen due to the strong relief of the area. The whole model was discretised in 224 x 144 x 192 cells resulting in a total amount of about 6.2 million cells.

The local model comprises a size of 9.5 x 12.5 x 6.5 km^3, discretised in cubic cells of a dimension of 50 m x 50 m x50 m. The lithology is built up by 10 lithological units already described in the geology section and contains 20 fault structures which have been inserted as additional units, guaranteeing a connection of the cells along the fault trace. Numerical stability and convergence of the model realizations is only achieved by sealing the fault structures to topography. Therefore we assume that the alluvial aquifer made up by basalts and other volcanic deposits is completely separated from the geothermal system in the local model by the ignimbrite seal. This seal is assumed to seal the fault structures on local scale as well.

4.2.2 Petrophysical properties

Parameterisation of the model cells is performed mostly using laboratory measurements done within GEMex on outcrop and reservoir sample plugs. Report D 6.1 explains in further details the final result of the complete measurements as well as details on the methods used. It is to be noted that many samples from outcrop locations suffered from weathering whereas reservoir samples show a strong hydrothermal overprint. Therefore the correlation of laboratory results to the expected rock compositions is very demanding. Additionally both, reservoir and outcrop samples show a high sampling bias. For the shallow units, unfortunately only few samples are available from outcrop and reservoir locations, so the representativeness of those samples might be questionable.

The petrophysical properties of porosity, matrix thermal conductivity (dry and saturated state), intrinsic permeability and volumetric heat capacity of the modeled units were obtained from laboratory measurements on core plugs from the Los Humeros and Las Minas area. The samples collected cover almost all available rock types in the area of the Los Humeros caldera. The assignment of the samples to particular units in the model is based on literature, visual identification of rock types and measured petrophysical properties.

For local model, with sub-units comprising of different rock types, the parameters per rock type obtained from the laboratory measurements are weighted equally, as their relative contributions to the local unit are not known in detail. Especially Unit 1 and Unit 2 are built up of several contrasting volcanic compositions, whose parameters are defined only by few samples from the preliminary data set. A similar procedure was used to calculate the properties of basement unit 9a, comprising mainly limestone accompanied by metamorphosed products of chert, marble and skarn. We assume the limestone to contribute to this basement section by 95% and the metamorphic compounds to contribute by an amount of 5% of the total rock volume

The regional model however comprises of broad groups classified based on temporal evolution of the caldera rather than the lithology. Therefore rock types with very different petrophysical and thermal properties are grouped together as one group. For parameterization, the petrophysical parameters of each sub-unit is weighed by its relative contribution to the corresponding chronological group. The weight is defined by averaging the thickness of a specific lithology unit from the wells. For this purpose, the labelled and subdivided units in wells reinterpreted in WP 3 are used.

Figures 6 – 10 are data obtained from laboratory measurements and are compiled within Task 6.1.

Matrix thermal conductivity: Figure 6 and Figure 7 shows the thermal conductivity measurements for dry and saturated andesite outcrop and andesite reservoir (CFE plugs) samples respectively. These measurements are used to calculate the value of matrix thermal conductivity, λ_m using the geometric mixing law (8). This law was proven to give a sufficiently accurate description of effective thermal conductivity of a rock and water mixture for rock types without foliation or schisting (Hartmann et al., 2005).

It is observed that the matrix thermal conductivity value for andesite obtained from measurements performed in the outcrop samples are very low as compared to the measurements performed in the reservoir samples from CFE core data (Figure 7). Matrix thermal conductivity calculated using geometric mixing law from the reservoir samples provides a much higher value of thermal conductivity for andesite. For parametrization, we use the values of TC matrix obtained from CFE reservoir andesite samples. This was due to the fact that the TC matrix obtained from the outcrop samples seems to strongly affected due to sample conditions as well as the samples suffer from severe alterations (details in D6.1 report). Figure 8 presents the measurements in all limestone samples. The average value and standard deviation of matrix thermal conductivity calculated using the measurements are used for parametrization for limestone units. Similar procedure is followed for all other rock types.

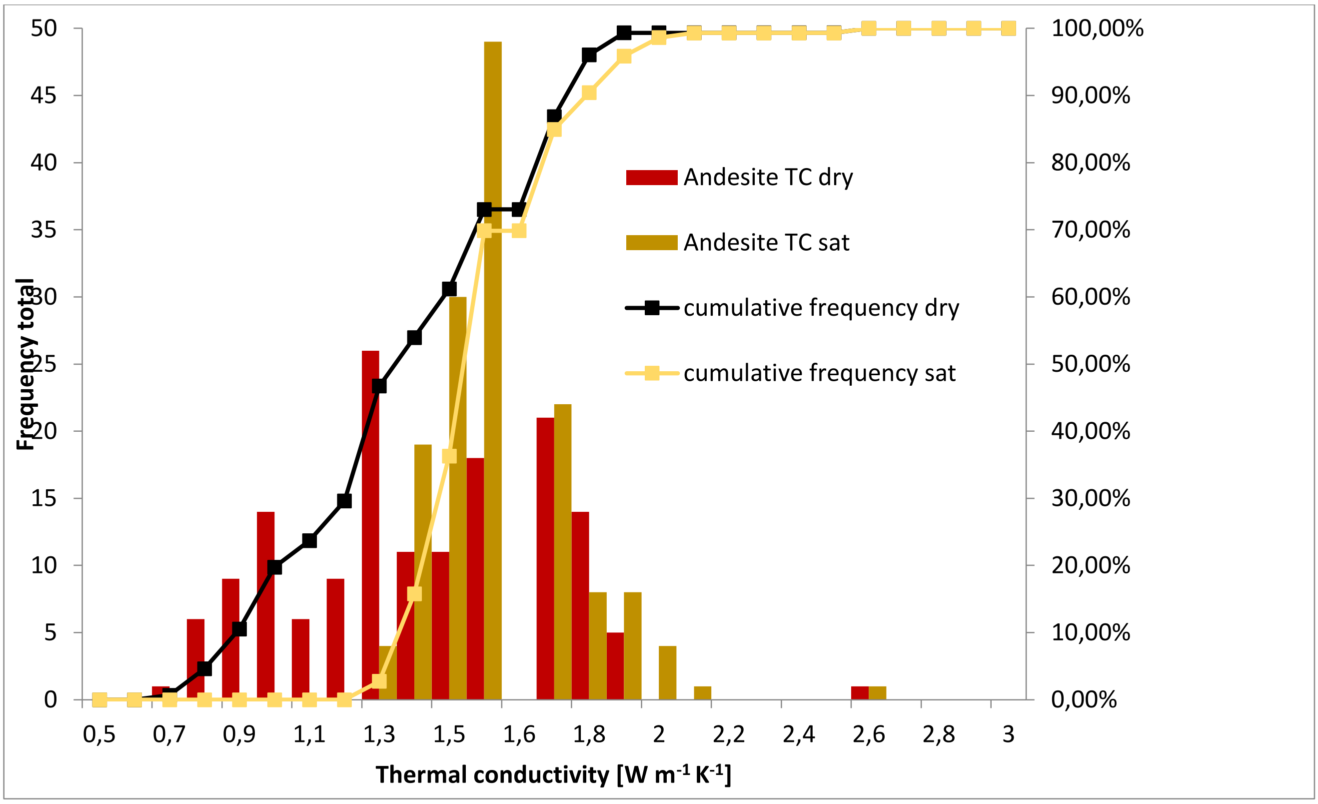

Figure 6: Thermal conductivity measurements for outcrop andesite samples in dry and saturated conditions (Task 6.1)

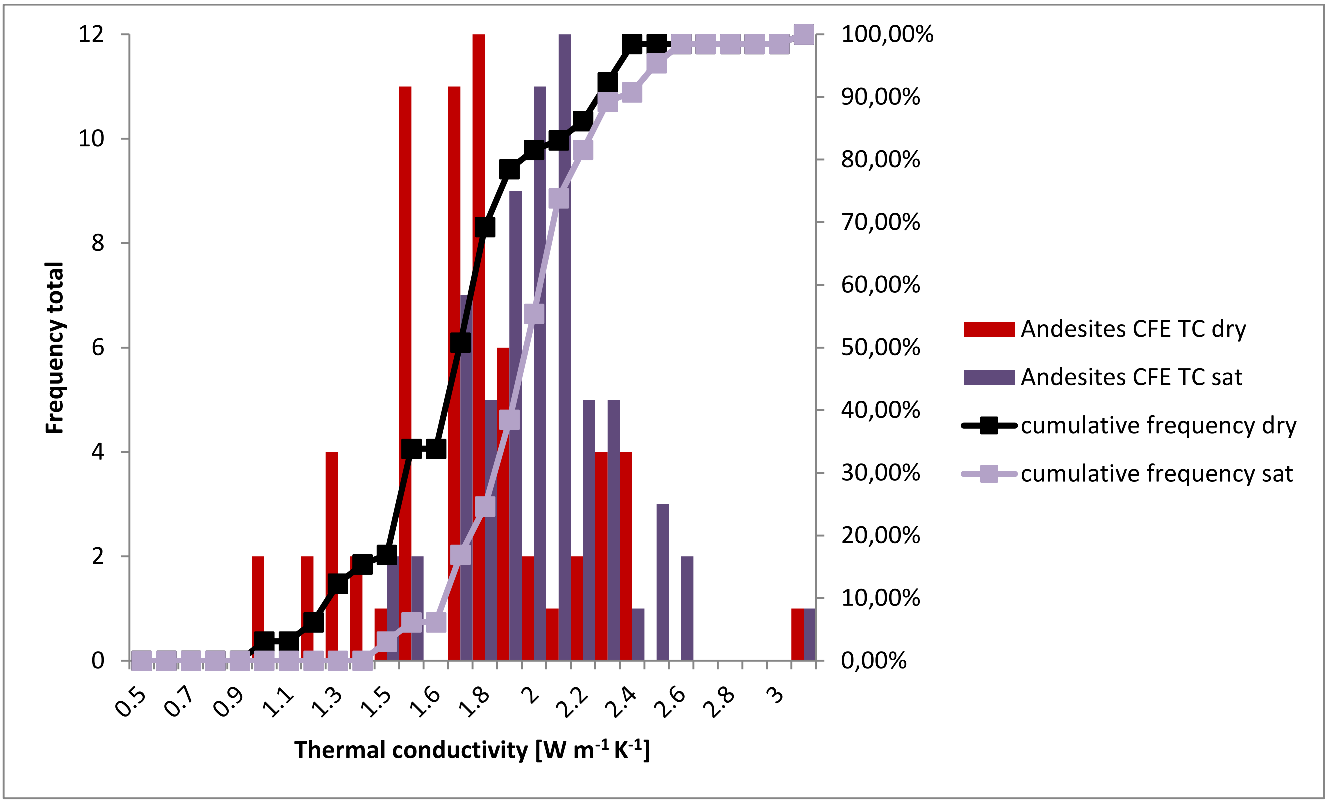

Figure 7: Thermal conductivity measurement for reservoir samples of andesite (Task 6.1)

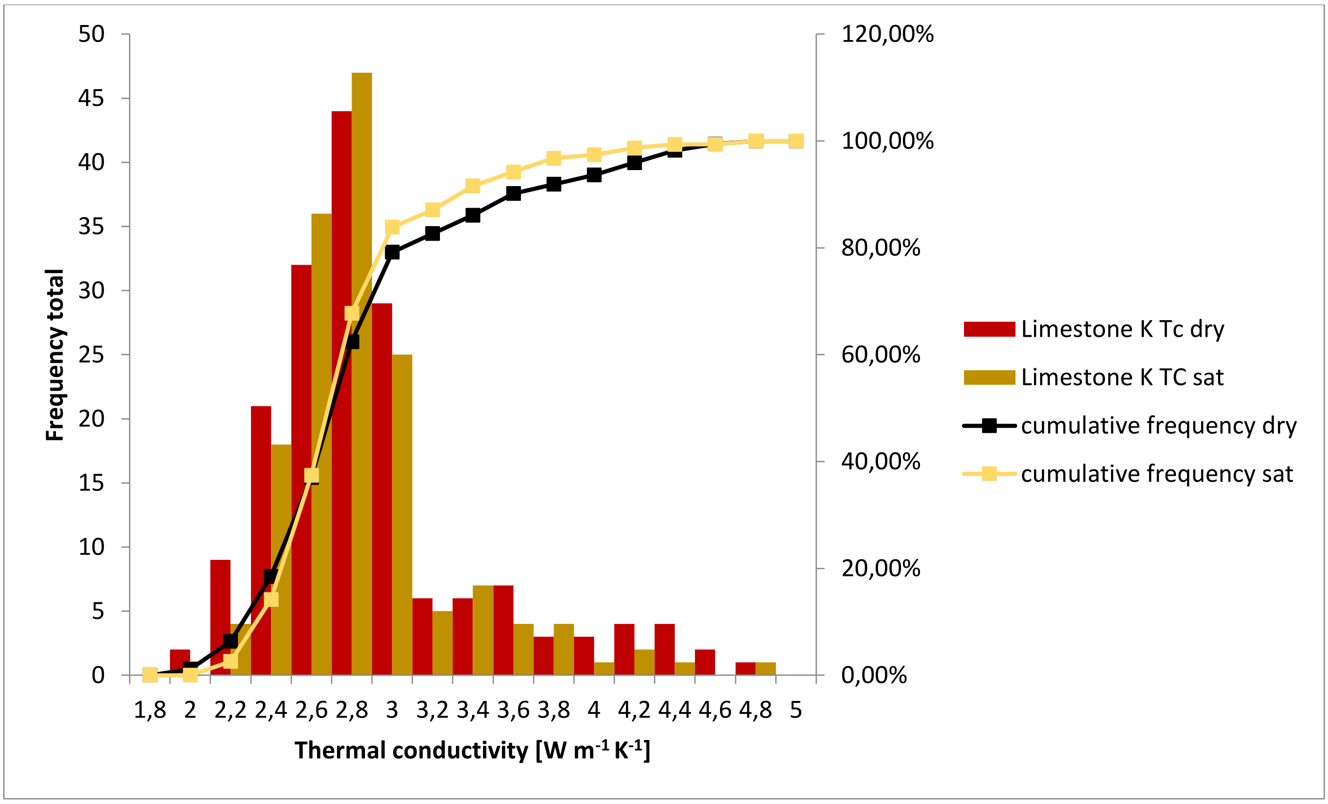

Figure 8: Thermal conductivity measurement for cretaceous limestone samples for dry and saturated conditions (Task 6.1)

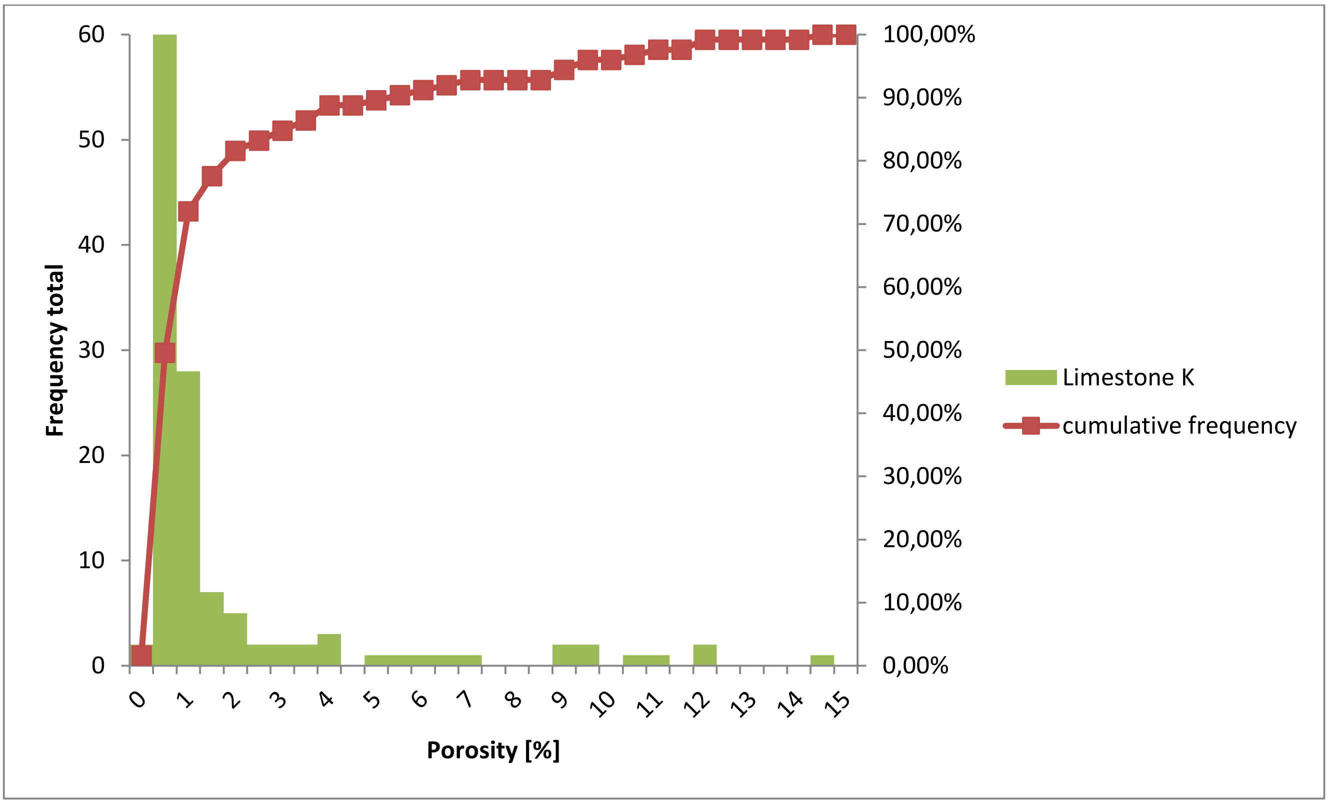

Figure 9: Porosity measurement for Cretaceous limestone samples (Task 6.1)

Porosity: Porosity is obtained from laboratory measurements on rock samples from outcrop and reservoir scale. Figure 9 and Figure 10 shows the porosity distribution for limestone and andesite samples respectively.

It can be seen that almost 90% of the limestone samples have porosity lower than 2%. Accordingly an average value and standard deviation is assigned for limestone samples.

For the reservoir andesite units, it is observed that the porosity varies widely from < 3% up to samples showing a porosity of about 25 %. This is observed in both outcrop data (Figure 10) as well as petrophysical log measurements performed in the andesite sections of well H-42. Figure 11 shows well logs in the andesite sections of wells H-42. The andesites do not show uniform response in the lithology logs throughout the identified andesite section. The sonic, neutron as well as resistivity log show very well correlated peaks in certain sections. This response might be as a result of highly porous or fractured sections of andesite. Combination of FMI (Formation Micro imager) data and Acoustic logging have been used by CFE to interpret open fractures present in these sections (Pulido, 2008). The high porosity sections indicated by the data might be indicative of open fractures. Porosity calculated using sonic data in this andesite section reveals similar nature of pores (Figure 12). Visual inspection of the petrophysical log data as well as porosity measured in andesite samples indicate that at least 30% of the andesite sections might contain these highly porous/ fractured sections while the rest are massive andesites (3%– 4% porosity). Under the assumption that this distribution of fractured and massive andesite proportions represents the entire andesitic reservoir, we calculate the average property for both U7 and U 8 units with 30% high porous units and 70% massive low porous andesite.

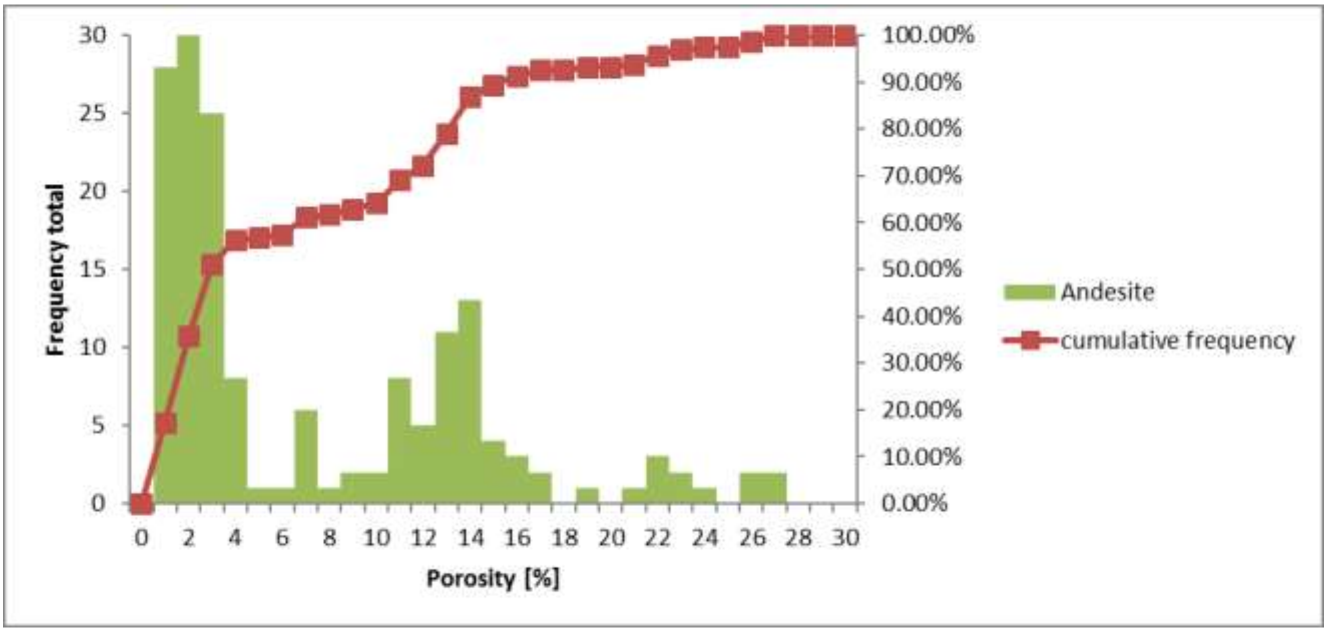

Figure 10: Porosity measured in all andesite samples

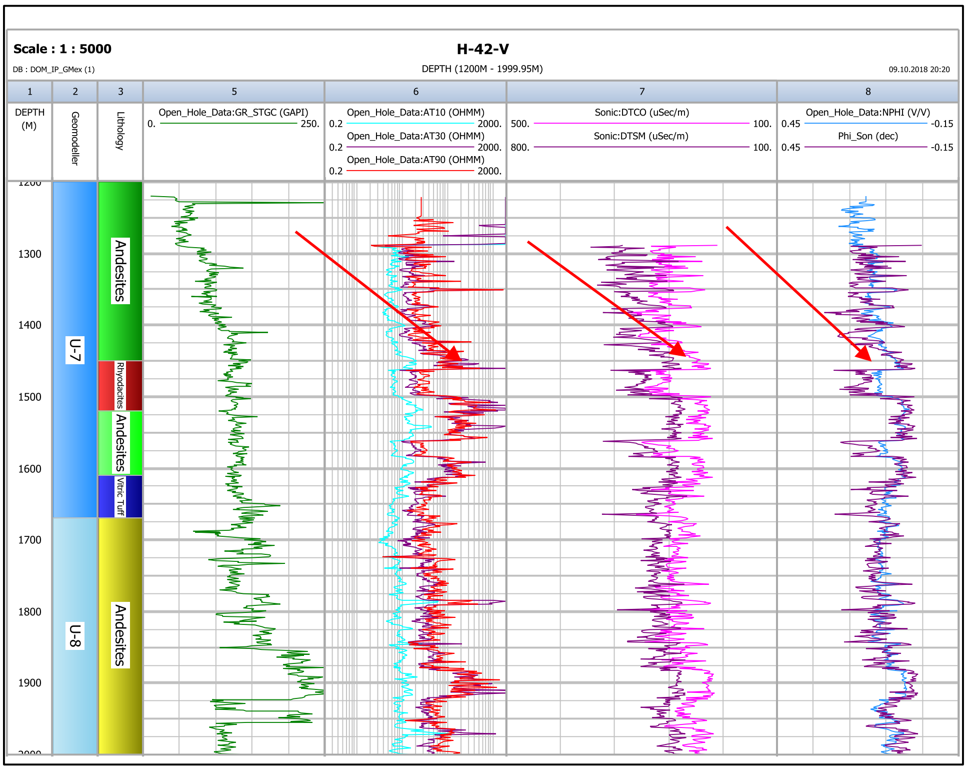

Figure 11: H 42 logging data from Andesite section, the red arrows indicate the consistent response of all the petrophysical logs towards the highly porous/fractured sections within the low porous massive andesites

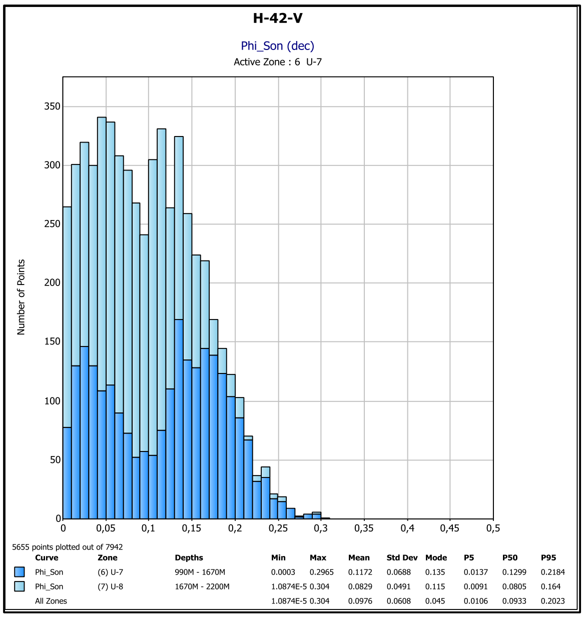

Figure 12: Distribution of porosity (sonic) within U 7 and U8 units from well H-42 sonic data

Matrix permeability: Intrinsic permeability calculated in the laboratory measurements are assigned to the units. As expected extremely low values of the order of 10^{-16} m^2 for andesites and 10^{-18} m^2 for limestones are obtained. This measurements corresponds to the matrix permeability and hence do not contribute much towards fluid flow within the reservoir. Table 3 shows the parameterization for every unit defined in the local model.

Table 3: Parameterization of the local units of the reservoir model

Lithology	Porosity [%]			Matrix Thermal Conductivity [W/(m K)]			Permeability (intrinsic) [m²]			Heat Production Rate [uW/m³]*	Volumentric heat capacity [J/(m³ K)]		
	Mean	Std. dev.	N	Mean	Std. dev	N	Mean	Std. dev	N	Mean	Mean	Std. dev	N
Unit 1: Pumice, ash fall deposits, some alluvium	50.01	1.00	5	1.91	0.10	5	1.27E-14	2.52E-15	5	0.5	2016751	22722	1
Unit 2: Basalts, Rhyodacites, Andesites, Olivine Basalts	12.80	2.60	19	2.18	0.23	11	1.18E-15	2.78E-15	16	0.5	2035034	79063	2
Unit 3: Zaragoza ignimbrites	14.30	1.96	15	2.74	0.13	14	1.17E-17	6.96E-18	10	1.48	2117271	154843	5
Unit 4: Rhyolitic and obsidian domes, fabby tuffs and andesitic - dacitic lava flows	12.13	0.60	4	2.31	0.12	3	8.00E-16	1.40E-15	6	1.5	1992487	151008	7
Unit 5: Xaltipan ignimbrites	14.30	1.96	15	2.74	0.13	14	1.17E-17	6.96E-18	10	1.48	2117271	154843	5
Unit 6: Rhyolites, dacites and few andesites and tuffs	12.13	0.60	4	2.31	0.12	3	8.00E-16	1.40E-15	6	1.8	1992487	151008	7
Unit 7: Pyroxene Andesites (30% porous/70% massive) ***	6.00	1.73	-	2.14	0.17	7	1.36E-16	1.12E-16	10	1.08	2140839	158948	16
Unit 8: Hornblende Andesites (30% porous/70% massive) ***	6.00	1.73	-	2.63	0.33	9	2.14E-16	1.79E-16	10	1.08	2127233	123154	13
Unit 9a: Limestones	2.02	1.96	28	2.77	0.17	20	3.00E-18	6.00E-18	24	0.62	2201903	195816	1
Unit 9a: Cherts/Marble/Skarn	1.44	1.53	32	4.20	0.56	20	6.80E-18	1.42E-17	[illegible]	0.62	2337680	427144	3
Unit 9a: Limestones 95% (Cherts/Marble/Scarn ~ 5%)	1.99	1.94	50	2.84	0.19	40	3.19E-18	6.41E-18	44	0.62	2208692	207382	4
Unit 9b: Granites/Granodiorites /Schists/Phyllites	2	1	-	3.2**	0.32**	-	3.00E-18	6.00E-18		2.45	2730075**	534374**	-

*(*compiled from literature values from Rybach (1876, 1986); **values for c_p and λ compiled from Schön (2004);*** bimodal distribution of porosity assumed, values calculated using a 70% massive, 30% porous rock mass). The deeper basement unit U9b was assumed to be of low permeability (no measurement available) using the same intrinsic permeability like for the upper basement unit U9a)*

For the regional groups the relative contribution of a specific local unit to a group was defined by computing the thickness of that unit divided by the total thickness of the modelled group in each well. This was evaluated based on the drilling record of all 50 wells. For consistency this evaluation was done by using the already labelled and subdivided preliminary dataset of lithological well record provided in the GeoModeller project. An example for the weighting process for Group I is given in Figure 13.

The obtained weights were used to define the properties of the broad regional groups. For all properties except the thermal conductivity the weighting was accounted for in an arithmetic manner. As we expect the volcanic system to have a horizontally layered structure with a perpendicular heat flow arrangement, the conductivity model can be described better by a model of thermal resistances in series, than by a model of parallel ones (Hartmann et al. 2005, Clauser 2011b). Therefore thermal conductivity for each group is derived from the harmonic mean, instead of the arithmetic one. For a total number of samples N with thermal conductivity λ the harmonic mean is given by:

$$\lambda_{harm} = \left(\sum_{i=1}^{N} \frac{n_i}{\lambda_i} \right)^{-1} \qquad (9)$$

In general all units have been parameterized in this manner. For Basement unit 9b, which is built up by schists, granites, granodiorites and phyllites, the values for the parameterization are compiled from literature due to unavailability of measurements for the respective rock types.

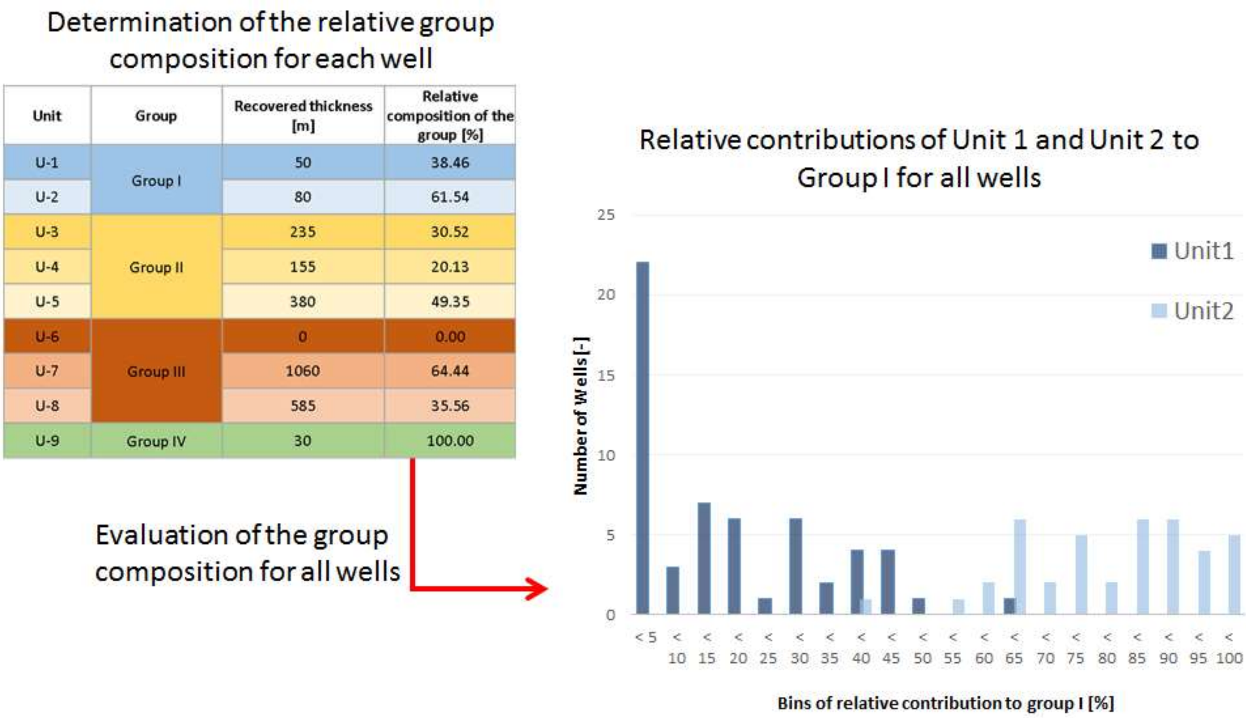

Unit	Group	Recovered thickness [m]	Relative composition of the group [%]
U-1	Group I	50	38.46
U-2		80	61.54
U-3	Group II	235	30.52
U-4		155	20.13
U-5		380	49.35
U-6	Group III	0	0.00
U-7		1060	64.44
U-8		585	35.56
U-9	Group IV	30	100.00

Figure 13: Workflow for determining weightage of units, example for Group 1 is shown

Table 4: Parameterization of regional model units

GROUP	PERCENTAGE of Unit in Group	UNIT	Porosity [%]	Thermal Conductivity Matrix $\left[\frac{W}{m\,K}\right]$	Permeability (intrinsic) [m^2]	Heat production rate* $\left[\frac{\mu W}{m^3}\right]$	Vol. heat capacity $\left[\frac{J}{m^3 K}\right]$
	MEAN [%]		Mean	Mean	Mean	Mean	Mean
GROUP 1	**15.59**	**1: Undefined pyroclastics**	50.01	1.91	1.27E-14	0.50	2016751
	84.41	**2: Post Caldera Lava Flows**	12.80	2.18	1.18E-15	0.50	2035034
	100.00		**18.60**	**2.13**	**2.98E-15**	**0.50**	**2032184**
GROUP2	**34.81**	**3: Los Potreros Caldera**	14.30	2.74	1.17E-17	1.48	2117271
	7.99	**4: Inter Caldera Deposits**	12.13	2.31	8.00E-16	1.50	1992487
	57.2	**5: Los Humeros Caldera**	14.30	2.74	1.17E-17	1.48	2117271
	100.00		**14.12**	**2.70**	**7.47E-17**	**1.48**	**2107300**
GROUP3	**3.86**	**6: Upper Pre-Caldera**	12.13	2.31	8.00E-16	1.80	1992487
	64.16	**7: Inter Pre-Caldera*** **	6.00	2.14	1.36E-16	1.08	2140839
	31.98	**8: Basal Pre-Caldera*** **	6.00	2.63	2.14E-16	1.08	2127233
	100.00		**6.24**	**2.28**	**1.86E-16**	**1.11**	**2130761**
GROUP4	**3000 m thickness**	**9a: Basment: Limestones**	2.02	2.77	3.00E-18	0.62	2201903
		Cherts/Marble/Skarn	1.44	4.20	6.80E-18	0.62	2337680
		Limestones 95% (Cherts/Marble/Scarn 5%)	**1.99**	**2.84**	**3.19E-18**	**0.62**	**2208692**
	Below 3000 m depth	**9b: Basement Granites, Granodiorites, Schists, Phyllites**	2.00	3.20**	3.19E-18	2.45	2730075**

*(*compiled from literature values from Rybach (1876, 1986); **values for c_p compiled from Schön 2004; *** bimodal distribution of porosity, values calculated using a 70% massive, 30% porous rock mass)*

4.2.3 Boundary conditions

In the following sections, we discuss workflow which is applied to the regional model for evaluating the boundary conditions for the reservoir model. The simulations for the reservoir model which will be discussed in Deliverable D 6.6.

At the top of the model domain, represented by the topographical surface, temperature was assigned depending on the air temperature gradient, resulting in decreasing temperature with altitude. From the CFE hydrogeological report, the average annual air temperature at Los Humeros climate station, which is located at an elevation of 2862 m.a.s.l. is 11.86 °C (CFE hydrogeological report). As no soil temperature is available from the station data, the boundary condition of temperature at the ground surface is calculated from the mean annual air temperature and the topographic height, assuming ground surface and air temperature has the same gradient. Los Humeros region can be classified after Köppen as subtropical highland climate (CFE hydrogeological report), verifying the use of a wet adiabatic temperature gradient in air of 0.00491 K m^{-1}. The difference between air and soil temperature can reach up to several degrees Celsius (Clauser, 1984) and vary transient in their amplitude (Smerdon und Stieglitz, 2006). This difference and the annual transient signal are not accounted for in our model. Compared to the uncertainties resulting from basal heat flow density, caldera geometry and flow processes in the target depth of 1000 m to 1500 m we expect them to be negligible for the model purpose.

Pressure at the topographic surface is assumed to be atmospheric, implying the groundwater surface and therefore the hydraulic head coinciding with the topographic surface. Groundwater flow as a result is driven by topography. As described in the conceptual model section, the recharge pathways and direction of fluid flow is not yet well established, however the infiltration and percolation might be possible through the distal outcropping limestone formations in the north western part of the caldera as well as through vertical infiltration within the caldera. Fluid pathways, direction of fluid flow as well as the ground water level cannot be determined from the piezo-metric well data (Rodríguez 2000). This is especially due to the impact of pressure depletion on the data a result of production.

The average specific heat flow obtained from borehole data in the TMVB and Sierra Madre Oriental is 90 mW m^{-2} (± 16 mW m^{-2}), (Ziagos et al. 1985). Other authors state the specific heat flow in the area to range between 75 mW m^{-2} and 83 mW m^{-2} (Pollack et al. 2010) or even 35 mW m^{-2} and 85 mW m^{-2}in the north of Los Humeros geothermal field (Davies 2013). This observed high variability of the heat flow distribution on a larger scale can be explained by the complex setting of the continental trench-arc-back arc system and the temperature perturbations due to uplift, orogeny and erosion (Ziagos et al. 1985). As Los Humeros Caldera is limited to the east by the Cofre de Perote volcanic chain and to the west by the Sierra Madre Oriental high, the specific heat flow from Ziagos et al. 1985 of 91 mW m^{-2} is taken as regional specific heat flow background signal for the TMVB. Assigning this specific heat flow condition to our model domain, could not reproduce the bottom hole temperatures of the coldest wells in the vicinity of the caldera (e.g. H-14). The heat signal(s) under the caldera complex overprints the regional heat flow pattern by at least one order of magnitude.

Being unsure of the exact depth, temperature, shape and the position of the heat source, as well as the cooling and recharge history, we tested different specific heat flow pattern shaped by the geometries of the caldera outlines using corrected bottom hole temperatures of the wells as calibration points.

4.2.3.1 Determining basal heat flow conditions

Temperature data is only available within the small outline of Los Humeros Caldera, which is not sufficient for estimation on regional scale. From the corrected bottom-hole temperature pattern of wells, it is evident that the specific heat flow of 91 mW m^{-2} (Ziagos et al. 1985) observed in the regional scale (TMVB) is not sufficient to model the temperature anomaly within the caldera system. The temperature data at the bottom of the wells indicate that there is no uniform heat flux under the caldera system but the heat signals are rather localised. In absence of any information on the shape and placement of magma pockets, we use a specific heat flow pattern, shaped by the caldera geometries at the bottom of our model domain. Therefore, in a first attempt, we consider four 2D E-W oriented cross sections, A-A’, B-B’, C-C’ and D-D’ (Figure 14) and perform simulations assuming a pure conductive model. The regional heat flow outside the Los Humeros caldera is taken to be 91 mWm^{-2} while the estimate of the specific heat flow at the bottom of the domain was obtained by a comparison of the simulation results to the corrected bottom-hole temperatures. For the initial simulations, we consider only the temperatures of the boundary wells as shown in Figure 14.

Wells H-14 and H-25 are assumed to be influenced by a pure conductive heat transport (Figure 15). These wells show no significant indication for advective heat transport and fluid loss zones from their temperature logs and drilling record shows simulated temperatures iteratively upscaling the specific heat flow boundary condition from 150 mWm-2 to 350 mWm-2 at the bottom of the regional model domain, within the outlines of Los Humeros caldera. Solid and dashed lines show the simulation results using the two different relationships of thermal conductivity and temperature proposed by Sekiguchi (1984) (solid lines) and Zoth and Hänel (1988) (dashed lines). The red point shows the corrected bottom-hole temperature of the well using Equation 1 and the black triangle gives the corrected bottom-hole temperature of the well using Equation 2. It is observed that the temperature simulated using both these two methods differ considerably with increasing specific heat flow and depth.

H-14 is located in the south of Los Humeros caldera rim and H-25 is the easternmost well of the field. The conductive simulations are performed using the thermal conductivity – temperature relationship of

Sekiguchi as explained in Section 4.1. Figure 16 presents temperatures extracted for wells H-14, H-5, H-25 and H-18 from 2D conductive simulations. Figure shows that wells H -14 and H-25 match the corrected bottom hole temperature with specific heat flow values between 225 mW m^{-2} and 250 mW m^{-2}. Well H-18 which is the southernmost well of Los Potreros caldera can be matched with a specific heat flow of around 275 mWm^{-2} whereas wells close to the N-S oriented main fault setting like H-5, H-2, H-21 and H-22 could not be matched conductively with values as high as 350 mW m^{-2}. H-5 shown here as an example.

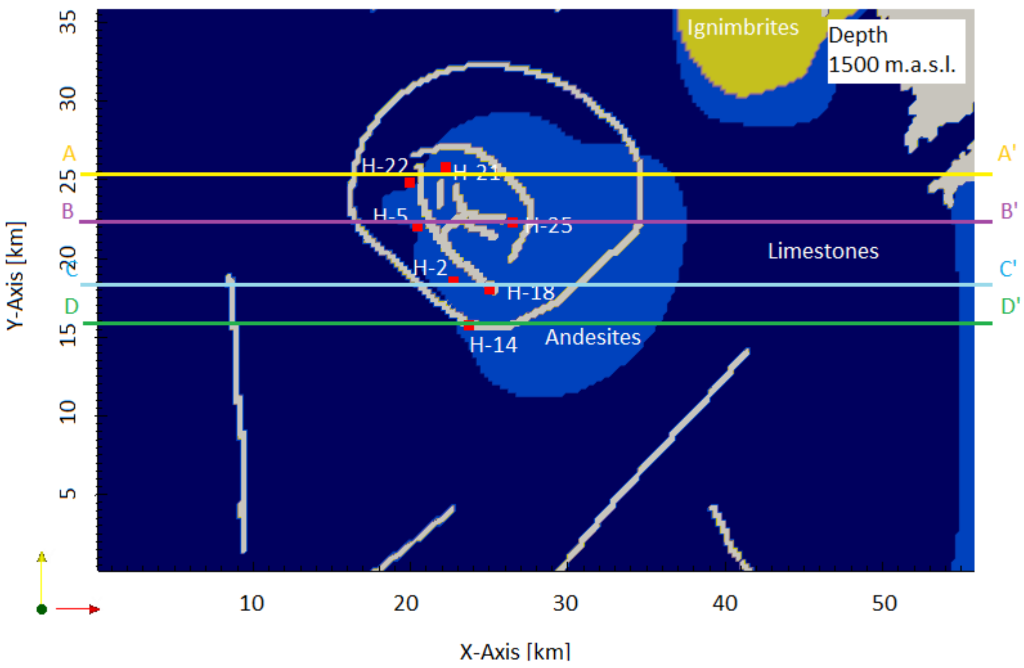

Figure 14: Cross-section A-A', B-B', C-C' and D-D' with boundary plotted in a lithology slice at a depth of 1500 m.a.s.l., the different colors in the slice indicate the lithology types modeled at that depth, the main fault system are outlined in white color, locations of the boundary wells are shown with red dots

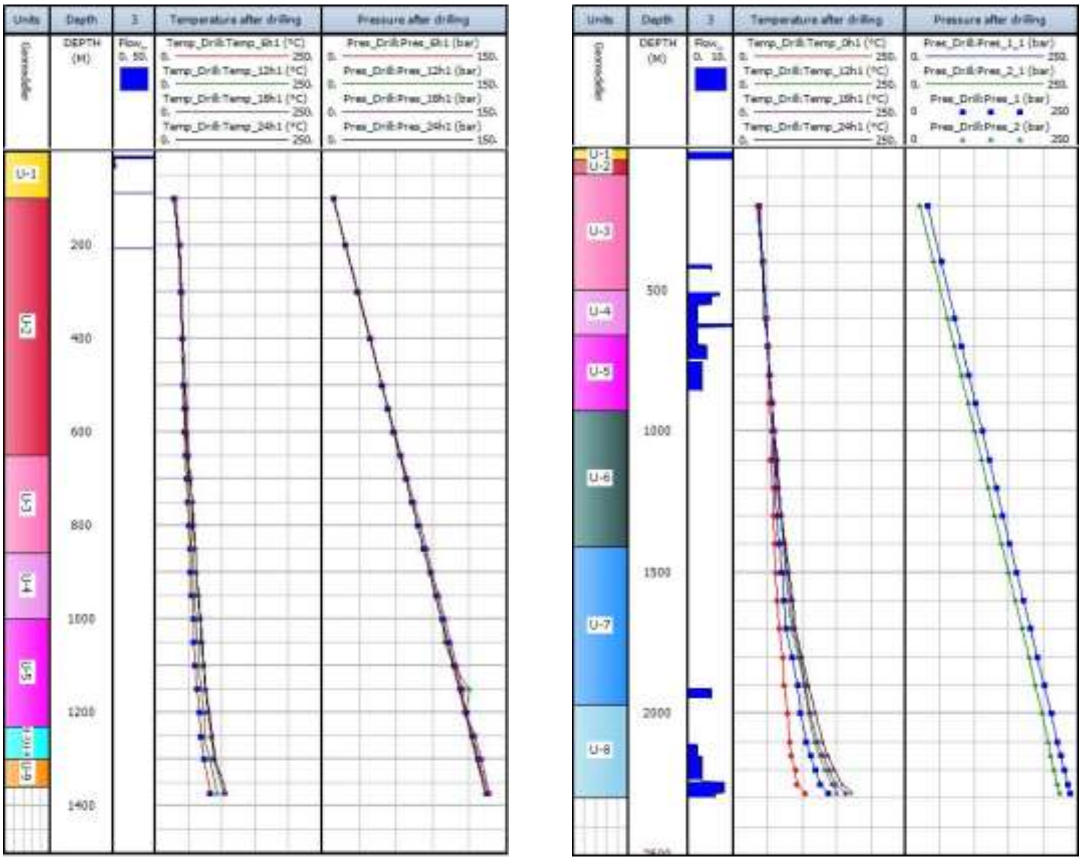

Figure 15: Temperature and pressure log of well H-14 and H-25

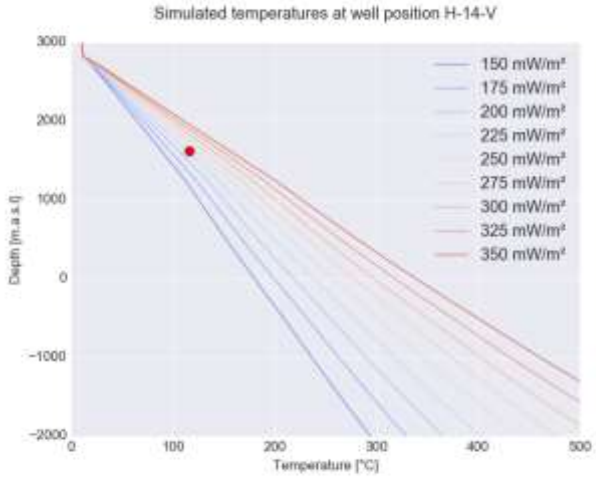
Simulated temperatures at well position H-14-V
150 mW/m²
175 mW/m²
200 mW/m²
225 mW/m²
250 mW/m²
275 mW/m²
300 mW/m²
325 mW/m²
350 mW/m²
Depth [m.a.s.l]
Temperature [°C]

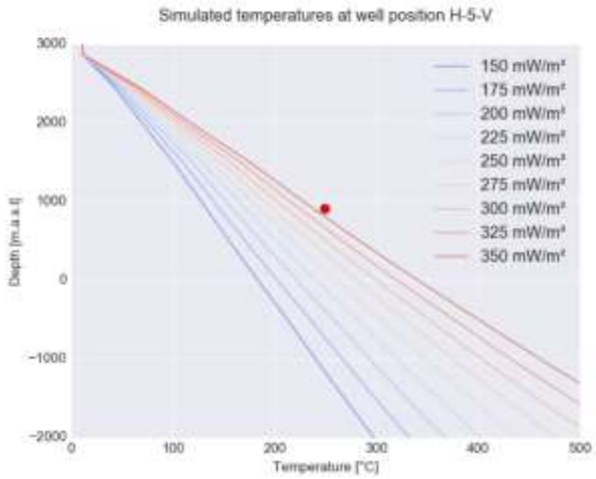
Simulated temperatures at well position H-5-V
150 mW/m²
175 mW/m²
200 mW/m²
225 mW/m²
250 mW/m²
275 mW/m²
300 mW/m²
325 mW/m²
350 mW/m²
Depth [m.a.s.l]
Temperature [°C]

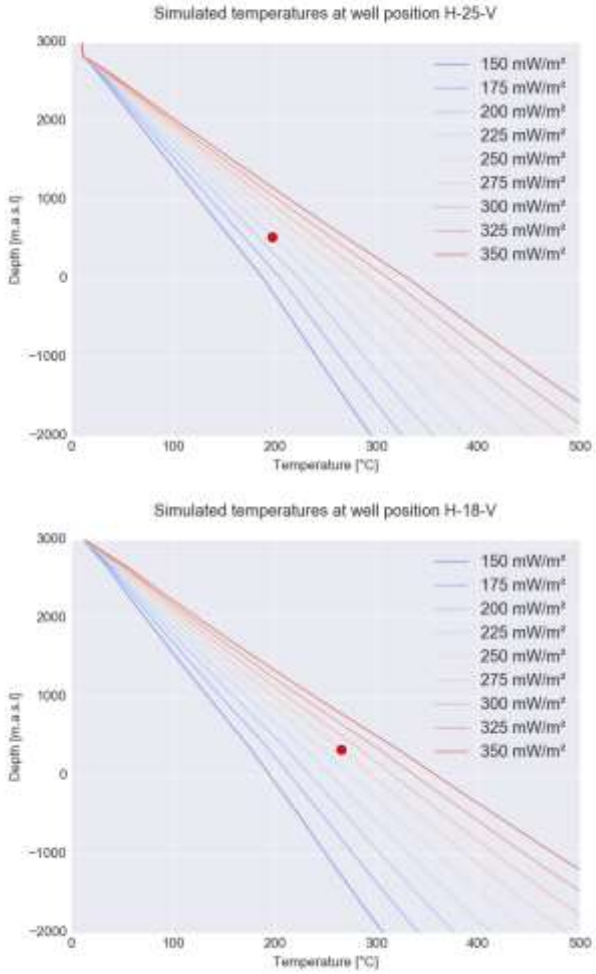

Figure 16: Temperature profiles from conductive simulations along 2D E-W cross-sections extracted for well H-14, H-5, H-25 and H-18; the red point shows the Horner corrected bottom-hole temperature for the respective wells

The 2D conductive simulations provided an initial estimate of the specific heat flow pattern. This pattern was then tested in the 3D regional configuration (Figure 17). As was evident from the initial simulations, that a uniform heat flow under the caldera complex is not sufficient to result in the complex temperature pattern we observe in the bottom-hole depths of wells, we decided to test several conductive scenarios by varying the basal heat flow pattern. Table 5 shows six different scenarios of the regional conductive model assuming possible heat flow configurations.

Figure 18 presents the comparison of different conductive scenarios along cross-section B – B', which crosses H-5 and H25 (Figure 17). With increasing specific heat flow from Scenario 1 to Scenario 5, isotherms are uplifted towards the caldera floor. Between Scenario 1 and Scenario 5 for example the uplift of the 500°C isotherm is about 1 km.

Table 5: Heat flow scenarios for testing basal heat flow conditions in the 3D regional model

Scenario	Regional specific heat flow	Los Humeros caldera	Los Potreros caldera	North-eastern part of Los Potreros caldera
	[Wm^{-2}]	[Wm^{-2}]	[Wm^{-2}]	[Wm^{-2}]
Scenario 1	0.091	0.175	0.225	0.225
Scenario 2	0.091	0.175	0.250	0.250
Scenario 3	0.091	0.175	0.250	0.350
Scenario 4	0.091	0.200	0.250	0.250
Scenario 5	0.091	0.200	0.300	0.300
Scenario 6	0.091	0.200	0.300	0.450

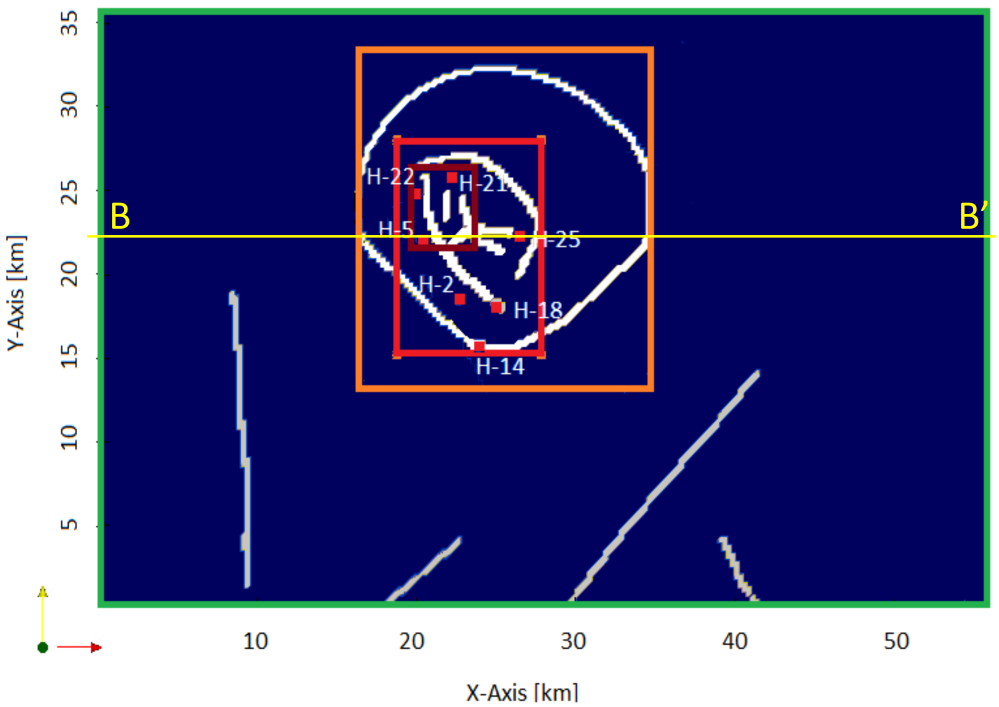

Figure 17: Specific heat flow pattern in the 3D model domain at 4600 m below sea level, green boundary: regional specific heat flow; within orange and red rectangles: the Los Humeros and Los Potreros caldera values, respectively. Within the dark red rectangle, the highest specific heat flow used in the north-eastern part of Los Potreros caldera (Table 1). The yellow line B-B' is a E-W cross section which is used for extracting temperature for visualisation.

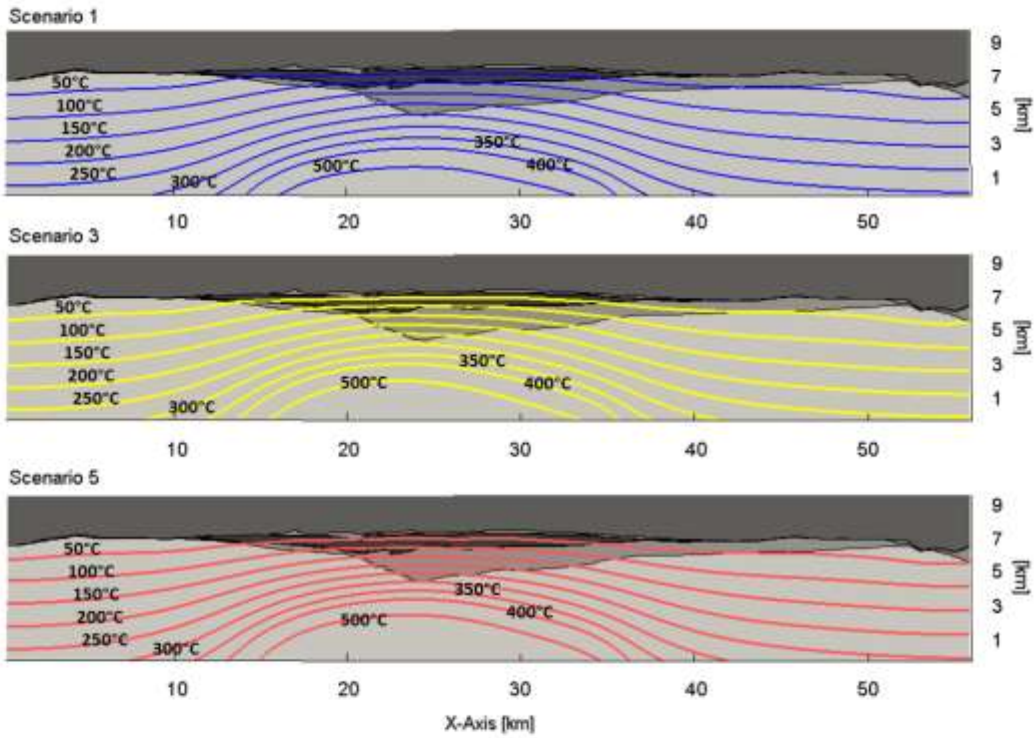

Figure 18: Comparison of isotherms for B-B' cross-section for different scenarios of 3D conductive simulations

Figure 19 shows the simulated temperatures extracted for four wells, H-14, H-18, H-25 and H-5 for the conductive scenarios presented in Table 5. We checked the match between the wells and the simulated temperatures and found out that none of our chosen configuration can explain all the data. Bottom-hole well temperatures corrected according to equations [1] and [2] are indicated by red circles and black triangles, respectively. At the reservoir level (1500 m a.s.l.) of well H-14, the southern-most well of the field, the different scenarios yield a spread in temperature on the order of 21 K. With depth the difference in resulting temperature increases for the different scenarios. But overall, a basal specific heat flow as high as 200 mW m^{-2} used in Scenario 4 and 5 under the Los Humeros Caldera seems appropriate.

The most easterly well of the Los Potreros caldera, H-25, requires a basal specific heat flow of the order of 225 mW m^{-2} – 250 mW m^{-2} for an acceptable match with the well data.

In contrast, the simulated temperatures of wells H-18 and H-5 could not be matched by any of the above configurations. Well H-5 shows a conductive trend in the temperature logs, and the drilling data show no indication of circulation losses at greater depth. Wells H-21 and H-22, located in the north-eastern part of Los Potreros caldera, cannot be matched even with a very high basal specific heat flow of the order of 450 mW m^{-2} (Scenario 6).

From the conductive model we obtain an idea of the specific heat source at the bottom of our domain which we will use for further investigations. We choose Scenario 5 for further investigation since the heat pattern used in this scenario provided a reasonable match to bottom hole temperature of most of the wells which shows a conductive pattern in the temperature response. This scenario however tends to underestimate the bottom hole temperature of many other central and northern wells. Increasing the heat capacity further in the northern eastern part of Los Potreros caldera to 350 mW m^{-2} (in Scenario 3) and 450 mW m^{-2} (in Scenario 6) , does not lead to better to match with the well data and causes instability in simulation. This leads to different theories for explanation, including on the one hand a strong advective heat transport processes happening along the faults and corresponding fracture networks and conductive heating of the surrounding, and on the other hand, a possible much shallower heat source, formed by local intrusions. In summary, the idea proposed in previous studies of one single magma body cooling underneath Los Humeros and Los Potreros caldera is seriously challenged by our analysis.

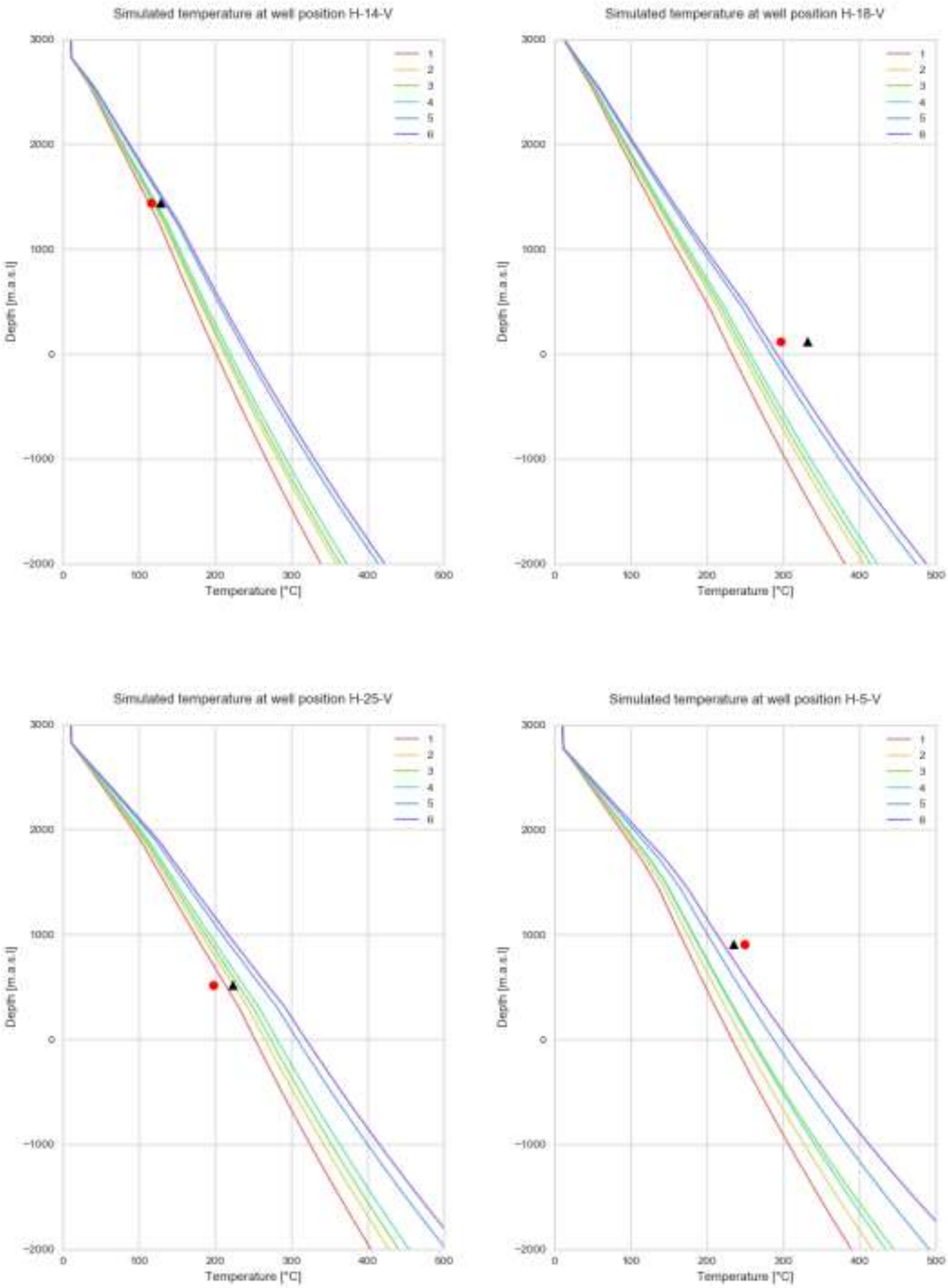

Figure 19: Simulated temperatures extracted for wells H-14, H-18, H-25 and H-5 for different conductive scenarios from 3D conductive modelling, red circle and black triangle indicates the bottom-hole well temperature corrected according to equations [1, Horner method] and [2, SRF], respectively.

4.2.4 Regional convective model

The conductive simulations confirmed the fact that the phenomenon of heat conduction alone is unable to explain the temperatures observed in the wells. It was necessary to include advection to evaluate the following aspects of the field:

I. to understand the influence of permeability contrasts on the recharge and flow pathways, especially for the most uncertain permeability of the limestone basement,
II. to evaluate the effect of open versus closed faults,
III. to have a better estimate of temperature and pressure conditions at the boundary of the local reservoir model.

Assuming this possibility of distal recharge, we tested the sensitivity of pressure and temperature of the boundary wells of the geothermal field for a range of limestone permeability varying from intrinsic (10^{-18} m^2) to 100 times intrinsic permeability (10^{-16} m^2).

Under the assumption of open fault system (not sealed due to mineral precipitation) within the caldera, the major fluid pathways are formed by the faults and related fractures which intersects the andesite units and probably the deeper limestone rocks at variable depths. Assigning appropriate hydraulic properties to the faults and fracture networks in this environment is very challenging. From laboratory measurements, only intrinsic permeability is available for the samples which contains no information of the secondary permeability created due to fractures of different scale. So, under the assumption that fluid flow in this geothermal system is primarily due to faults and related fractures, we use information from pressure transient analysis to have an initial indication of fault permeability. Aragón et al. (2008), Sánchez Luviano et al. (2015) evaluate the damage zones of different wells from their production data (pressure, enthalpy, etc.) and provide an estimation of the permeability of the damaged zone. We use this information to parametrise the fault zones.

Another unknown configuration is given by the fault-setting of the caldera rims. From the conceptual point of view, it is also unknown whether the caldera rim faults are open or closed to flow, and therefore open or closed to lateral recharge and recharge from topography. We tested the following three different fault configurations:

1. Los Humeros Caldera rim and Los Potreros Caldera rim impermeable to flow,
2. Los Humeros Caldera rim closed to flow and Los Potreros Caldera rim open to flow,
3. Los Humeros Caldera rim and Los Potreros Caldera rim open to flow.

From the geological point of view a fourth possible combination of Los Humeros caldera rim open to flow and Los Potreros caldera rim closed to flow is very unlikely due to the older age of Los Humeros Caldera. The three fault scenarios were combined with another possible implication resulting from flow anisotropy. Within the limestone basement it can be expected that flow will happen preferentially in horizontal direction, due to the layered structure of this rock unit. Within the reservoir andesite, we can expect flow to happen preferentially in z-direction due to the steep normal faulting, and corresponding fracturing. To account for these possibilities, we combined the fault scenarios with an anisotropy assumption for permeability resulting in six regional model scenarios. From each of the models we extracted the boundary conditions for the local model (Table 6).

For all other magmatic and metamorphic modelling units the average intrinsic permeability was used. Limestone and andesite matrix permeability as obtained from laboratory measurements are 10^{-18} m^2 and 10^{-16} m^2 respectively. Scenario 1a and 1b, for example assume that both LH and LP caldera faults are sealed and therefore they are assigned 10^{-17} m^2. In Scenario 2a and 2b, the faults within the LP caldera are open to flow and are assigned 10^{-15} m^2, one order of magnitude higher than that of the surrounding reservoir rocks (andesite).

Table 6: Permeabilities and permeability anisotropy factors for different fault sealing conditions used in this study (anisotropy factor in z-direction is 1)

Scenario	LH rim perm [m²]	LP rim perm [m²]	Fault perm inner caldera [m²]	Limestone anisotropy factor x-, y-direction		Andesite anisotropy factor x-, y-direction	
Scenario 1a	2.0×10^{-17}	2.0×10^{-17}	3.0×10^{-15}	1	1	1	1
Scenario 1b	2.0×10^{-17}	2.0×10^{-17}	3.0×10^{-15}	2	2	0.5	0.5
Scenario 2a	2.0×10^{-17}	2.0×10^{-15}	3.0×10^{-15}	1	1	1	1
Scenario 2b	2.0×10^{-17}	2.0×10^{-15}	3.0×10^{-15}	2	2	0.5	0.5
Scenario 3a	2.0×10^{-15}	2.0×10^{-15}	3.0×10^{-15}	1	1	1	1
Scenario 3b	2.0×10^{-15}	2.0×10^{-15}	3.0×10^{-15}	2	2	0.5	0.5

5 Results and Discussion

5.1 Recharge and Permeability

Recharge to the Los Humeros geothermal reservoir is believed to take place mostly within the caldera (Cedillo-Rodriguez, 2000). Due to the massive ignimbrite layer sealing the caldera outline, the infiltration of meteoric water is possible through firstly, the faults and fracture networks provided they are not sealed due to mineralisation and secondly, through shallow porous volcanic deposits in areas where sealing layers do not exist. These constraints provides strong limitations to recharge options from meteoric water. Production fluids from wells H-1, H-1D and H-12 do not contain atmospheric nitrogen, but rather a deep CO_2 enriched component indicating that the source of the fluid is somewhere deeper where volcanic-hydrothermal interactions occur (Arellano et al., 2015). Cedillo-Rodriguez (2000) also suggested the upward vertical recharge for magmatic fluids through faults and fractures.

Distal recharge, if any, from outside the caldera might only be possible through the fractured outcrops which must run deep enough and have connected pathways to reach the bottom of the geothermal reservoir at depth of between 1000 m.a.s.l. – 1300 m.a.s.l. Fractured limestone outcrop to the northwest of Los Humeros Caldera occurs and the general topographic gradient might favour inflow from this direction, however the change in permeability of these fractured limestone with depth is unknown. The matrix permeability of the limestone as measured from outcrop samples is on the order of 10^{-18} m^2 and in absence of fractures or dissolution structures at depth, they are almost impermeable.

If the deep annular faults of the caldera rim are sealed and closed to flow, then the distal recharge may not be able to enter the geothermal reservoir. It is difficult to simulate all the variable situations which might occur if the faults are impermeable or permeable or partially permeable. We tried to test three different possibilities for the major fault configurations as mentioned in Section 4.2.4. In addition, we tested the recharge conditions by varying limestone permeability.

In the following paragraphs, we discuss results from one of the most probably scenarios – Scenario 3a, where we consider all the major faults are open and contributing to flow. The limestone and andesite matrix permeability considered for simulation are 10^{-18} m^2 and 10^{-16} m^2 respectively. Both Los Humeros rim fault and Los Potreros rim faults along with the other regional faults are open to flow with permeability, 10^{-15} m^2.

In Figure 20, Darcy velocity and hydraulic head extracted along a W-E cross-section and S-N cross section passing through the center of Los Humeros as well as Los Potreros caldera. Because of the very low permeability of the host rocks, most of the recharge takes place through the high permeability fault rims (10^{-15} m^2). This is indicated by the larger magnitude of the Darcy velocity arrows in the faults as compared to the rocks.

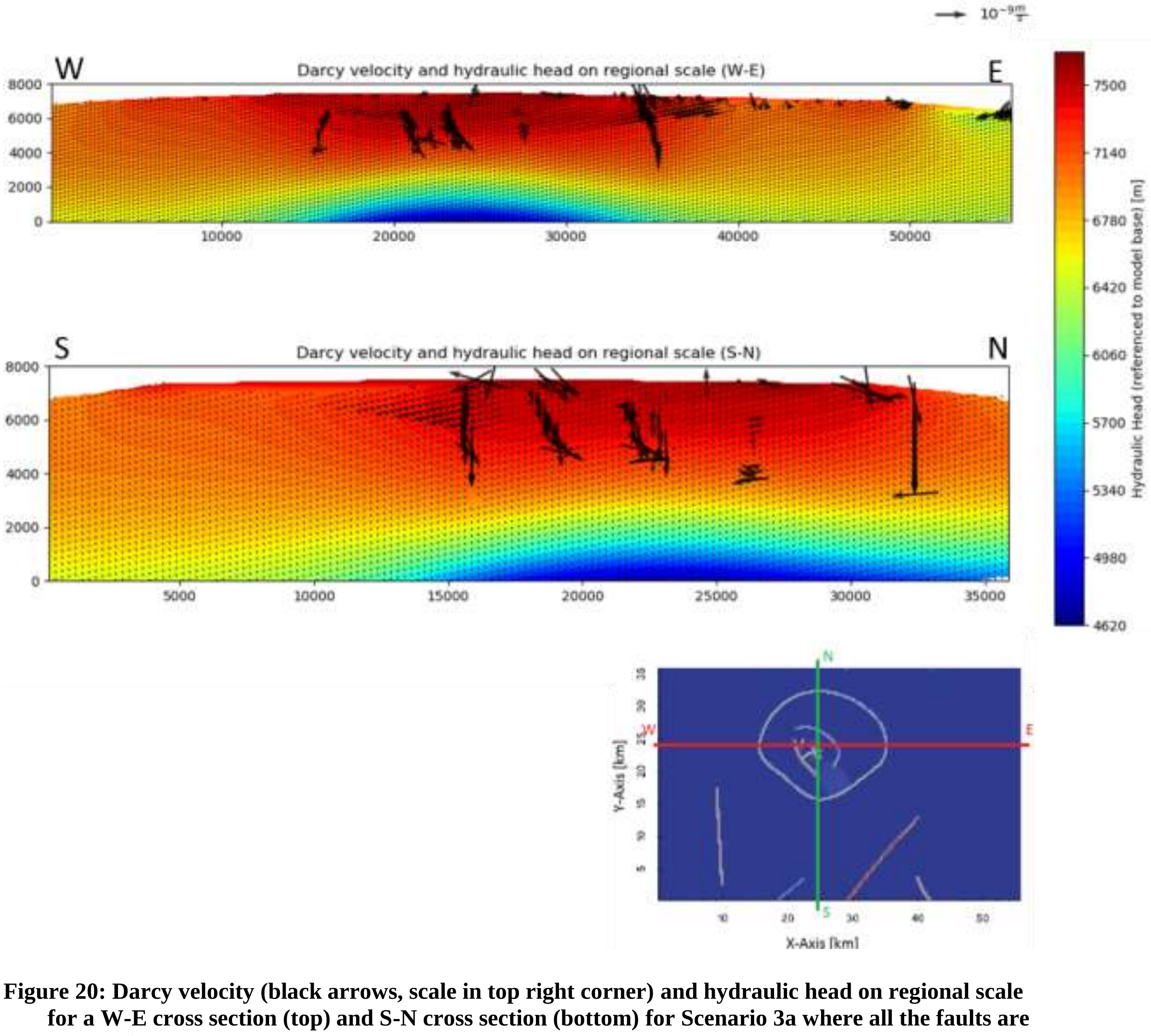

Figure 20: Darcy velocity (black arrows, scale in top right corner) and hydraulic head on regional scale for a W-E cross section (top) and S-N cross section (bottom) for Scenario 3a where all the faults are open to flow, the cross section positions are shown below in the bottom right w.r.t. to Los Humeros caldera fault boundaries (outlined in white),

To better understand, the flow situation at the reservoir depth, we extracted the Darcy velocity and hydraulic head at 1500 m.a.s.l (Figure 21). The zone of interest in the figure is outlined with the black dashed boundary. The north-east and the south-west corner of the plot suffers from boundary effect. However these boundary problems do not affect our zone of interest. The fluid movement is essentially driven by topography and it can be observed that outside the caldera, the flow velocities are very low and the dominant heat transport mechanism is conduction while within the caldera faults and particularly towards the south-east of caldera, convection plays a dominant role.

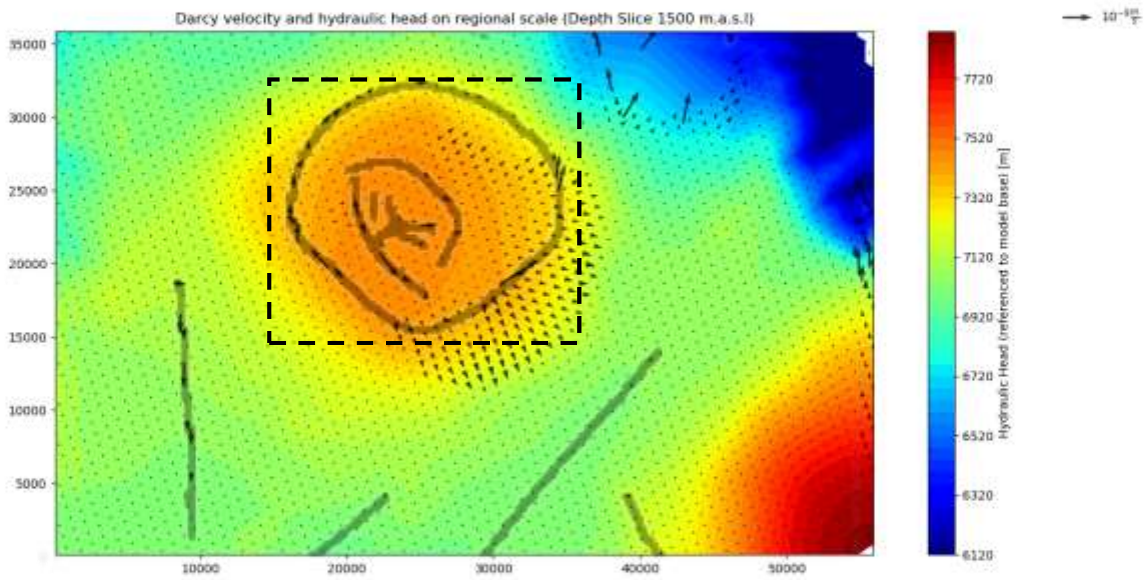

Figure 21: Darcy velocity (black arrows, scale in top right corner) and hydraulic head on regional scale at 1500 m.a.s.l. with all faults open and contributing to fluid flow, the dashed black boundary indicates the zone of interest, the very high and low hydraulic heads observed in the south-east and north-west corner in the plot is a boundary effect and is out of the zone of interest.

Additional scenarios: Increasing Limestone and Andesite permeability

In Figure 22, we present scenarios considering increased limestone and andesite permeability. The idea behind is to evaluate the influence of increased limestone permeability towards fluid flow at the subsurface. In Figure 22, the intrinsic permeability of limestone as well as andesite is increased by one order of magnitude, i.e., limestone permeability is changed to 10^{-17} m^2 while and andesite to 10^{-15} $m^{2.}$ It can be observed that the fluid flux towards east and south-east of the caldera increases massively when limestone permeability is increased. However no significant change is observed towards the western part of the caldera. This implies that even if the limestone permeability is increased throughout the model, it does not lead to significant recharge towards Los Potreros caldera from the north-eastern side of the caldera where fractured limestone outcrops (Figure 3).

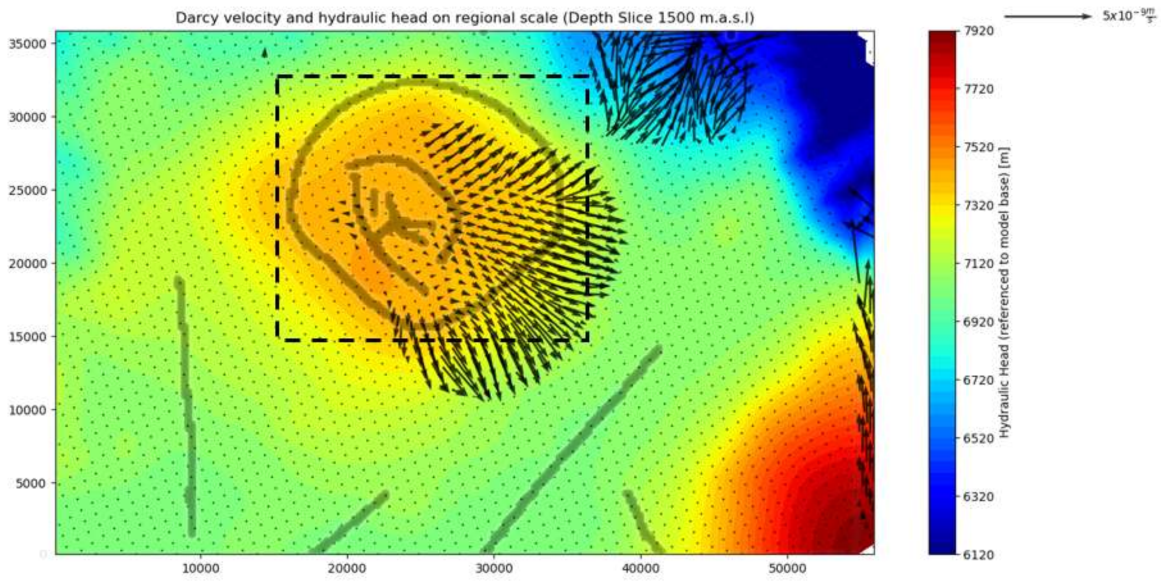

Figure 22: Darcy velocity (black arrows, scale in top right corner) and hydraulic head on regional scale at 1500 m.a.s.l. with Los Humeros fault closed to fluid flow but the rest faults are open, intrinsic limestone permeability of limestone increased to 10^{-17} m^2 and andesite to 10^{-15} m^2, the dashed black boundary indicates the zone of interest, the very high and low hydraulic heads observed in the south-east and north-west corner in the plot is a boundary effect and is out of the zone of interest.

5.2 Temperature models

From the modelled simulations, we obtained the temperature fields resulting from pure conductive as well as advective heat transport for the various scenarios. In Figure 24, temperature distribution for depth slices extracted at 1500 m.a.s.l. for convective simulation of Scenario 3a is presented. The drop in temperature in the south-east corner in Figure 23 is created as a result of the outcropping of modelled andesite along with thinning or complete absence of the sealing ignimbrite, which leads to a strong influx of cold water in this zone. At a depth of 1500 m.a.s.l., the minimum and maximum temperature ranges from 186 °C in the regional domain outside the caldera to 270 °C in the north-eastern part of the field.

From simulations performed using different convective scenarios, we obtain different temperature field distributions. In order to quantify the differences created due to the different configurations in the temperature field, we extract at particular depths, temperature distributions from all the scenarios. Figure 24 and 25, presents the mean temperature and standard deviation of all convective scenarios at depths of 1500 m.a.s.l. and 1000 m.a.s.l. respectively. The highest uncertainty in temperature is observed at the south eastern corner of the Los Humeros caldera fault (indicated with an arrow in Figure 24). With deeper depths (1000 m.a.s.l.), the standard deviation increases to almost 30 °C. However one of the main conclusions from all the convective scenarios above is that the rim fault of Los Humeros caldera plays a significant role in deciding the influx of cold water in the south-eastern part of the field.

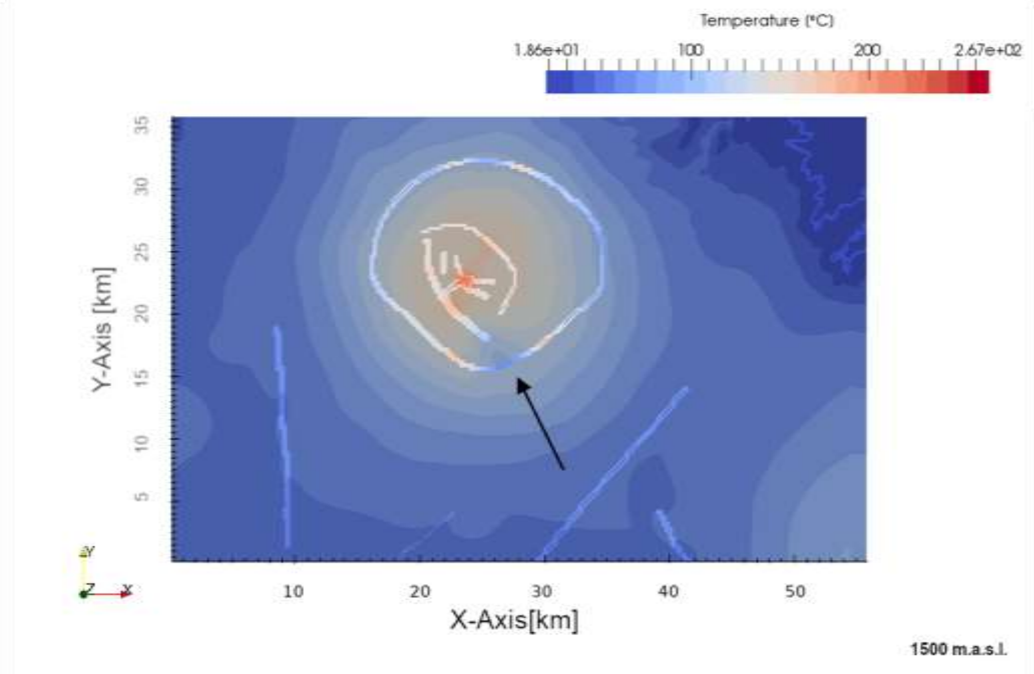

Figure 23: Temperature at 1500 m.a.s.l. for convective scenario 3a according to Table 6 where all the faults are open to flow, the black arrow points to the zone where maximum temperature uncertainty occurs due to different fault sealing configurations

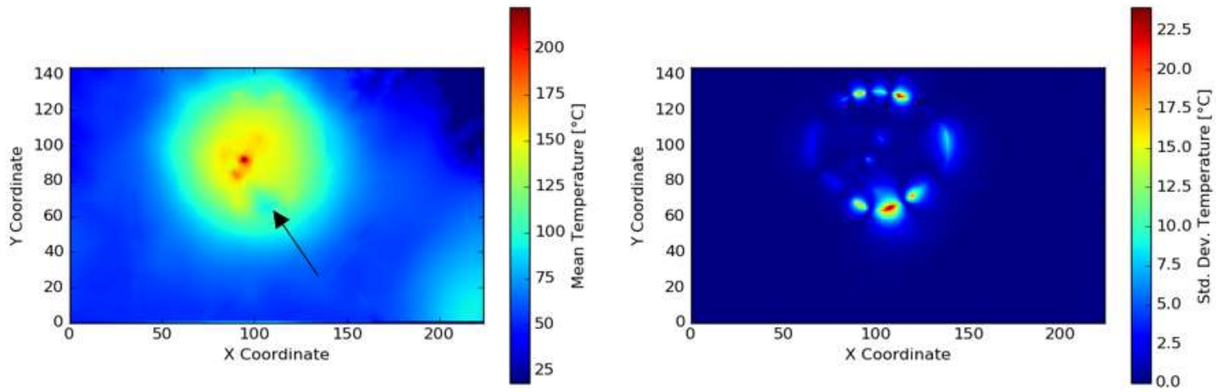

Figure 24: Temperature map - mean (left) and standard deviation (right) for all convective scenarios for depth 1500 m.a.s.l., the black arrow in the south-east corner of the field indicates the position where maximum uncertainty in temperature occurs.

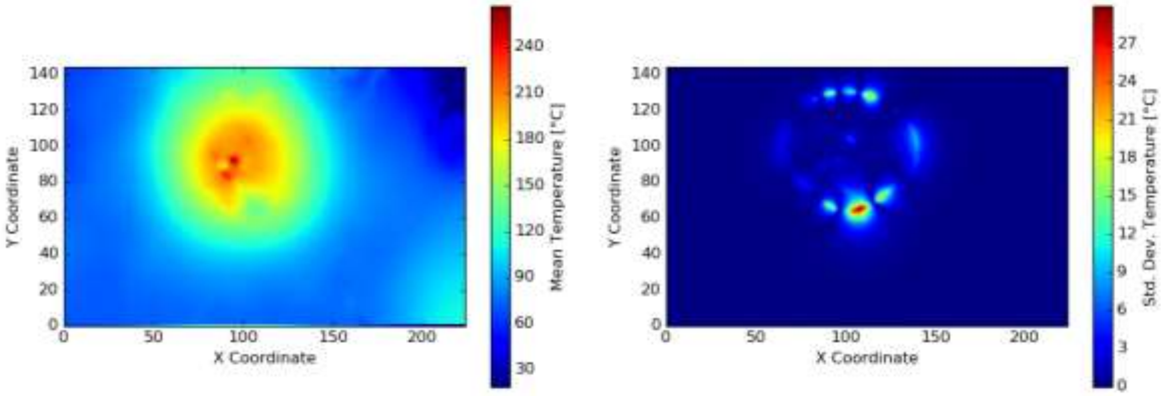

Figure 25: Temperature map - mean (left) and standard deviation (right) for all convective scenarios for depth 1000 m.a.s.l.

An overlay of isotherms from pure conductive (in red) and convective (in yellow) models is shown in Figure 26 for cross-section B-B’ defined in Figure 17. For the convective case, Scenario 3b is chosen for display (in yellow) where both Los Humeros and Los Potreros caldera rim faults are open to flow with permeability of the order of 2×10^{-15} m^2 (1 Md). Although the shapes of the isotherms are similar in both cases, the temperature difference between the conductive and convective isotherms differs by some tens of degrees at the same depth. This effect is prominent below ca. 1 km depth from surface. The effect of high permeability faults can be seen along the fault trace as compared to the host rock with permeability of the order of 10^{-16} m^2 (0.1 Md). Within the caldera system, the isotherms are even more disturbed due to the upwelling and the down flowing zones. Figure 27, shows a cross section B-B’ for specific heat flow where similar observations can be made in the center of the caldera where many faults intersect each other and heat transport is enhanced.

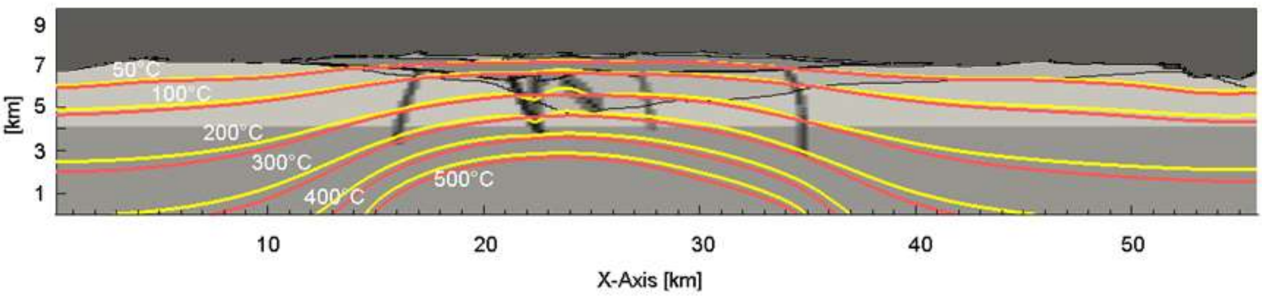

Figure 26: Comparison of isotherms for conductive and convective simulation for Scenario 3a along B-B’ cross-section

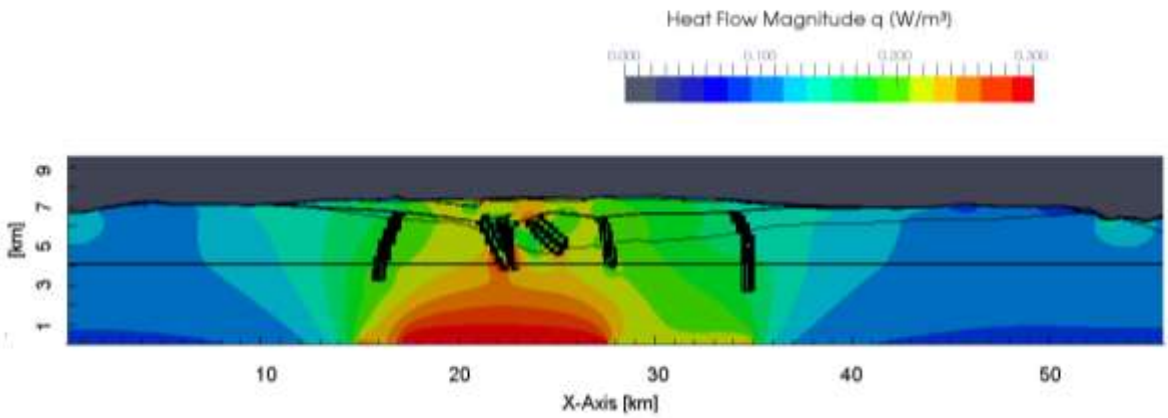

Figure 27: Heat flow magnitude along B-B' cross section for Scenario 3b of regional convective model

6 Conclusion

The numerical simulations presented in this report is performed on the regional model of size 56 x 36 x 12 km^3 for determining reasonable initial boundary conditions for a reservoir model of size 9.5 x 12.5 x 12 km^3. In general, it is possible to perform numerical simulation with assumptions of boundary conditions in fields where a priori information is available for certain parameters. Los Humeros, on the other hand, still lacks information on the fundamental conceptual ideas of the geothermal system. The conductive simulations provide an initial estimate of the heat flow conditions under the caldera complex. Regional convective models were important to understand the impact of unknown or assumed hydraulic properties of the structural elements on the regional temperature and pressure distribution. Important conclusions from the above study are:

- The current study is performed using a preliminary model of WP 3; the structural model including the rock units and most importantly lateral as well as vertical position of the faults strongly effects the upwelling and the down flowing zone. Comparing the simulated temperatures based on this structural model and carefully selected assumptions about rock and fault thermal and transmissive properties does not still provide a satisfying fit to all temperature observations from boreholes.

- Heat flow pattern under the caldera complex has been assigned in a simple upscaled pattern, however, temperature data in wells indicate a more complex pattern of heat distribution at depth. A much shallow and localised heat source is suspected towards the norh-eastern part of the field. Results of other investigations including high-resolution geophysical data could provide essential input to modify shape and dimension of possible heat source within the caldera complex. However, reliable information on the distribution of small scale heat sources is yet not available.

- Sealing conditions of faults and their permeability is essential for accurate modeling of recharge and production scenarios. We investigated the effects of these uncertainties on temperature and pressure distribution by simulating some possible scenarios. Investigation of different permeability scenarios resulted in six sets of boundary conditions which take into account the variable permeability of the faults and their structural setting. By combining the results of the various scenarios in the sense of a mean field and standard variations we are able to estimate the temperature uncertainty related to the unknown transmissivity conditions of the fault systems.

- The six different convective scenarios give six different set of boundary conditions. In the next report, numerical simulation will be performed using these sets of boundary conditions for the reservoir scale model. Presence of temperature and pressure data of the wells within Los Potreros caldera will be used for calibrating the model. Production data from numerous Los Humeros wells will be used to define the hydraulic parameters in more details.

7 Acknowledgements:

We thank the Comision Federal di Electricidad (CFE) for providing data and information regarding their geothermal wells and the entire GEMex consortium comprising of Mexican and European partners for the cooperation and unpublished inputs on conceptual ideas which are used for this study.

Laboratory measurements used in this study are performed in Task 6.1 within WP 6 and we would like to thank all Task 6.1 partners (TUDA, UNITO, GFZ, BGS) who contributed to the field work, sample collection, measurements and data analysis.

8 References

Aragón, A., Moya, S.L., García-Gutiérrez, A., Arrelano, V., 2008. A new method of damage determination in geothermal wells from geothermal inflow with application to Los Humeros, Mexico. *Geofísica Internacional, 47(4),* 371 – 382.

Arrelano, V. M., García, R.M., Barragán, G., Izquierdo, A., Araagón, A., Nieva, D., 2003. An updated conceptual model of the Los Humeros geothermal reservoir (Mexico), *Journal of Volcanology and Geothermal Reserarch , 124*, 67- 88.

Arellano, V. M., Barragán, R. M., Ramírez, M., López, S., Paredes, A., Aragón, A., Tovar, R., 2015. The Response to Exploitation of the Los Humeros (México) Geothermal Reservoir. *Proceedings World Geothermal Congress 2015, Melbourne, Australia.*

[Ascencio, F., Garcia, A., Rivera, J. and Arellano, V., 1994. Estimation of undisturbed formation temperatures under spherical-radial heat flow conditions. *Geothermics*, *23, 4*, 317-326.

Campos-Enríquez, J. O., Arredondo-Fragoso,J. J., 1992. Gravity study of Los Humeros caldera complex, Mexico: Structure and associated geothermal system, *Journal of Volcanology and Geothermal Reserarch, 49,* 69 – 90.

Calcagno, P., Evanno, g., Trumpy, E., Gutiérrez-Negrín, L. C., Macías, J. L., Carrasco-Núñez, G., Liotta, D., 2018. Preliminary 3-D geological models of Los Humeros and Acoculco geothermal fields (Mexico) – H2020 GEMex Project., *Advances in Geosciences, 45,* 321 – 333.

Carrasco-Núñez, G., López-Martínez, M., Hernández, J., Vargas, V., 2017. Subsurface stratigraphy and its correlation with the surficial geology at Los Humeros geothermal field, eastern Trans-Mexican Volcanic Belt, *Geothermics, 67,* 1 – 17.

Cedillo-Rodríguez, F, 2000. Hydrogeologic model of the geothermal reservoirs from Los Humeros, Puebla, Mexico. *Proceedings World Geothermal Congress 2000, Kyushu – Tohoku, Japan, May 28 – June 10, 2000.*

Estudio geohidrológico C.G. Los Humeros, 2015, CFE

Clauser, C., 1984. A climatic correction on temperature gradients using surface temperature series of various periods. *Tectonophysics, 103,* 33 – 46.

Clauser, C., 1992. Permeability of crystalline rocks. *EOS, Transactions American Geophysical Union, (73),* 233 – 238.

Clauser, C., ed., 2003. *Numerical Simulation of Reactive Flow in Hot Aquifers. SHEMAT and PROCESSING SHEMAT,* Springer, New York.

Clauser, C., 2011a. Thermal Storage and Transport Properties of Rocks, II: Heat Capacity and Latent Heat, In: Gupta, H. (ed.), *Encyclopedia of Solid Earth Geophysics,* Springer, Berlin.

Clauser, C., 2011b. Thermal Storage and Transport Properties of Rocks, II: Thermal Conductivity and Diffusivity, In: Gupta, H. (ed.), *Encyclopedia of Solid Earth Geophysics,* Springer, Berlin.

Davies, J. H., 2013. Global map of solid Earth surface heat flow. *Geochem. Geophys. Geosyst., 14,* 4608 – 4622.

de Marsily, G., 1986. *Quantitative Hydrogeology: Groundwater Hydrology for Engineers.* Academic Press.

Dowdle, W. L. and Cobb, W.M., 1975. Static formation temperature from well logs – an empirical method, *Journal of Petroleum Technology 27 (11)*, 1326-1330

Evans, J. P., Forster, C. B., Goddard, J. V., 1997. Permeability of fault-related rocks, and implications for hydraulic structure of fault zones, *Journal of Structural Geology, 19(11),* 1397 – 1404.

Eppelbaum, L.V. and Kutasov, I.M., 2006. Determination of formation temperatures from temperature logs in deep boreholes: comparision of three methods, Journal of Geophysics and Engineering, 348 – 355.

Ferriz, H. and Mahood, G.A. 1984. Eruption rates and compositonal trents at Los Humeros Volcanic Center, Puebla, Mexico. *Journal of Geophysical Research 89(B10),* 8511 – 8524, *doi: 10.1029/JB080i010p08511.*

García-Gutiérrez, A., Arellano, V., Barragán, R.M. Espinosa-Paredes, G. 2002, Initial temperature field in the Los Humeros geothermal reservoir, *Geofisica International, 41, 3*, 303-312.

García-Palomo, A., Macías, J. L., Tolson, G., Valdez, G., Mora, J. C., 2002. Volcanic stratigraphy and geological evolution of the Apan region, east central sector of the Trans-Mexican Volcanic Belt. *Feofísica Internacional, 41(2),* 133 – 150.

Giordano G., Lucci F., Rossetti F., Urbani S. 2018. Update on the volcanological conceptual model of Los Humeros geothermal field, *3rd GEMex Meeting, Morelia*

Hartmann, A., Rath, V., Clauser, C., 2005. Thermal conductivity from core and well log data. *International Journal of Rock and Mechanics & Mining Sciences, 42,* 1042 – 1055.

Horner D. R., 1951. Pressure buildup in wells, in Proceedings of Third World Petroleum Congress, Section II, The Hague, Netherlands, 28 May – 6 June.

Heap, M. J., Kennedy, B. M., Exploring the scale-dependent permeability of fractured andesite. *Earth and Planetary Science Letters, 447,* 139 – 150.

Norini, G., Groppelli, G., Sulpizio, R., Carrasco-Núñez, G., Dávila-Harris, P., Pellicioli, C., Zucca, F., De Franco, R., 2015. Structural analysis and thermal remote sensing of the Los Humeros Volcanic Complex: Implications for volcano structure and geothermal exploration. *Journal of Volcanology and Geothermal Research, 301,* 221 – 237.

Lee, Y., Deming, D., 1998. Evaluation of thermal conductivity temperature corrections applied in terrestrial heat flow studies. *Journal of Geophysical Research, 103(B2),* 2447 – 2454.

Lopez-Hernandez, A., 1995. Estudio Regional Volcanico y Estructural del Campo Geotermico de Los Humeros, Pue., Mexico. *Geoterm. Rev. Mex. Geoenerg. 11 (1),* 17–36.

Pardó M., Suárez, G., 1995. Shape of the subducted Rivera and Cocos plates in southern Mexico: Seismic and tectonic implications. *Journal of Geophysical Research, 100(B7),* 12357 – 12373: *doi:10.1029/95JB00919.*

Pasquale, V., Verdoya, M., Chiozzi, P., 2017. *Geothermics Heat Flow in the Lithosphere*, 2nd edition, SpringerBriefs in Earth Sciences, Cham, Switzerland. doi: 10.1007/978-3-319-52084-1

Pollack, H. N., Hurter, S. J., Johnson, J., R., 2010. Heat flow from the earth's interior: Analysis of the global data set. *Review of Geophysics, 31*, 267-280.

Pulido, C. D. L., 2008. Borehole Geophysics and Geology of well H-43, Los Humeros Geothermal Field, Puebla, México. *Geothermal Training Programme Report, 23 (2008), Orkustofnun, Grensásvegur 9, IS-108 Reykjavík, Iceland*

Rath, V., Wolf, A., Bücker, M., 2006. Joint three-dimensional inversion of coupled groundwater flow and heat transfer based on automatic differentiation: sensitivity, calculation, verification, and synthetic examples, *Geophys. J. Int.*, *167,* 453 – 466.

Roure, F., Alzaga-Ruiz, H., Callot, J.-P., Ferket, H., Granjeon, D., Gonzalez-Mercado, G. E., Guilhaumou, N., Lopez, M., Mougin, P., Ortuno-Arzate, S., Séranne, M., 2009. Long lasting interactions between tectonic loading, unroofing, post-rift thermal subsidence and sedimentary transfers along the western margin of the Gulf of Mexico: Some insights from integrated quantitative studies, *Tectonophysics, 475*, 169 – 189.

Rybach, L., 1976. Radioactive Heat Production: A Physical Property Determined by the Chemistry of Rocks, In: Strens, R. G. J. (ed.), *The Physics and Chemistry of Minerals and Rocks*, 309 – 318, Wiley & Sons, London

Rybach, L., 1986. Amount and Significance of Radioactive Heat Sources in Sediments, In: Burrus, J. (ed.), *Thermal Modelling in Sedimentary Basins, Editions Technip*, 311-322.

Sánchez Luviano, M., Armenta, M. F., Montes, M. R., 2015. Thermal Stimulation to Improve the Permeability of Geothermal Wells in Los Humeros Geothermal Field, Mexico. *Proceedings World Geothermal Congress 2015, Melbourne, Australia.*

Schön, J. H., 2004. *Physical Properties of Rocks: Fundamentals and Principles of Petrophysics*, 1. Edition, Elsevier, Amsterdam.

Sekiguchi, K., 1984. A method for determining terrestrial heat flow in oil basin areas. *Tectonophysics, 103,* 67 – 79, Elsevier Science Publishers B. V. Amsterdam – Netherlands.

Smerdon, J. E., und Stieglitz, M.,2006. Simulating heat transport of harmonic temperature signals in the Earth's shallow subsurface: Lower boundary of sensitivities, *Geophys. Res. Lett., 33,* L14402, doi: 10.1029/2006GL026816.

Suter, M., 1984. Cordilleran deformation along the eastern edge of the Calles-San Luis Potosí carbonate platform, Sierra Madre Oriental fold thrust belt, east-central Mexico. *Geological Society of America Bulletin, 95,* 1387 – 1397.

Verma, S. P., 1985. Heat source in Los Humeros geothermal area, Puebla, Mexico. *Transactions of the Geothermal Resource Council, 9,* 521 – 525.

Verma, S. P., Gómez-Arias, E., & Andaverde, J. (2011). Thermal sensitivity analysis of emplacement of the magma chamber in Los Humeros caldera, Puebla, Mexico. *International Geology Review*, 53(8), 905-925.

Wagner, W., Cooper, J., Dittmann, A., Kijima, J., Kretzschmar, H., Kruse, A., Mares, R., Oguchi, K., Sato, H., Stocker, I., Sifner, O., Takaishi, Y., Tanishita, I., Trubenbach, J., Willkommen, T., 2000. The IAPWS industrial formulation 1997 for the thermodynamic properties of water and steam. *J Eng Gas Turbines Power Trans ASME. 2000, 122(1),* 150–82. doi:10.1115/1.483186.

Ziagos, J. P., Blackwell, D. D., Mooser, F., 1985. Heat Flow in Southern Mexico and the Thermal Effects of Subduction. *Journal of Geophysical Research, 90*, 5410 – 5420.

Zoth, G., Hänel, R., 1988. Appendix: 10.1. Thermal Conductivity. In: Hänel, R., Rybach, L., Stegna, L., (eds.), Handbook of terrestrial heat flow density determination, Kluwer Academic Publishers, Dordrecht, pp 447 – 468.

Coordination Office, GEMex project
Helmholtz-Zentrum Potsdam
Deutsches GeoForschungsZentrum
Telegrafenberg, 14473 Potsdam
Germany